Electronic Supplementary Material (ESI) for Physical Chemistry Chemical Physics.

Hydrogen-Migration Governed Dynamic Magnetic Coupling Characteristics in Nitrogen-Vacancy-Hydrogen Nanodiamonds

Yamin Song, Xuexing Lin, Shaofen Yu, Yuxiang Bu, Xinyu Song*

School of Chemistry and Chemical Engineering, Shandong University, Jinan 250100, People's Republic of China

Supporting Information

Contents

1. Structural Character and Calculation Details

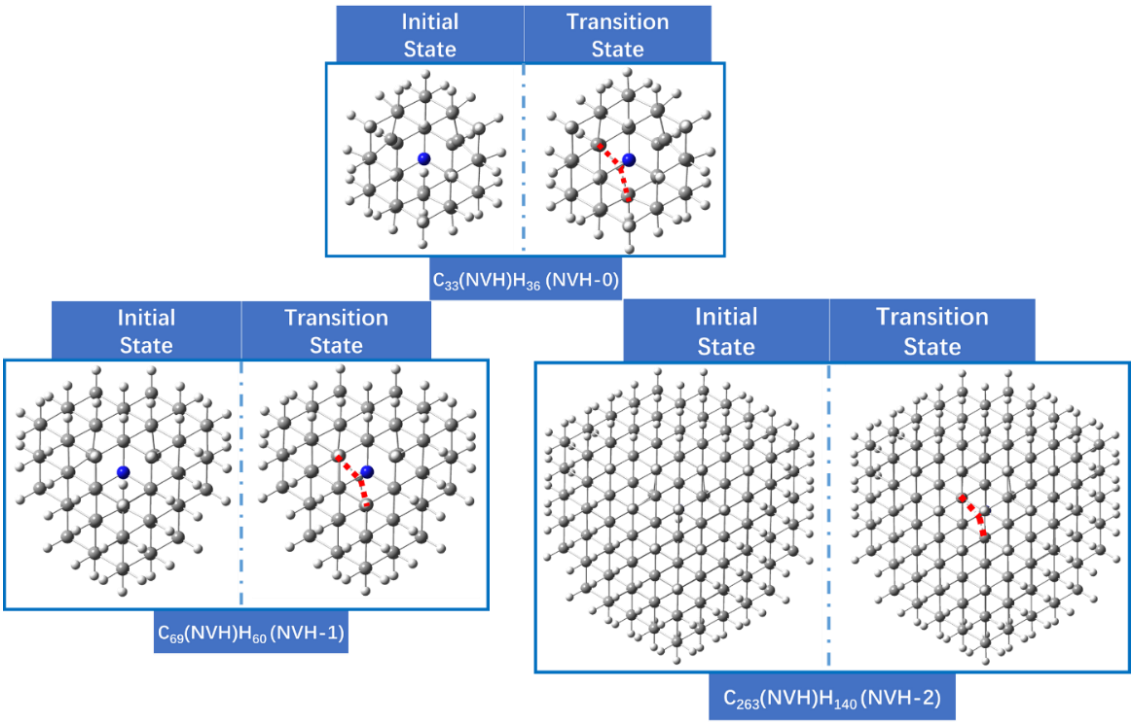

Figure S2. Three sizes of $C_{33}(NVH)H_{36}$ (NVH-0), $C_{69}(NVH)H_{60}$ (NVH-1), and $C_{263}(NVH)H_{140}$ (NVH-2) diamond nanoclusters in the initial state (Int) and transition state (TS), respectively. The H atom is bonded with C_1-radical in Int and in the middle of C_1 and C_2 radicals in TS.

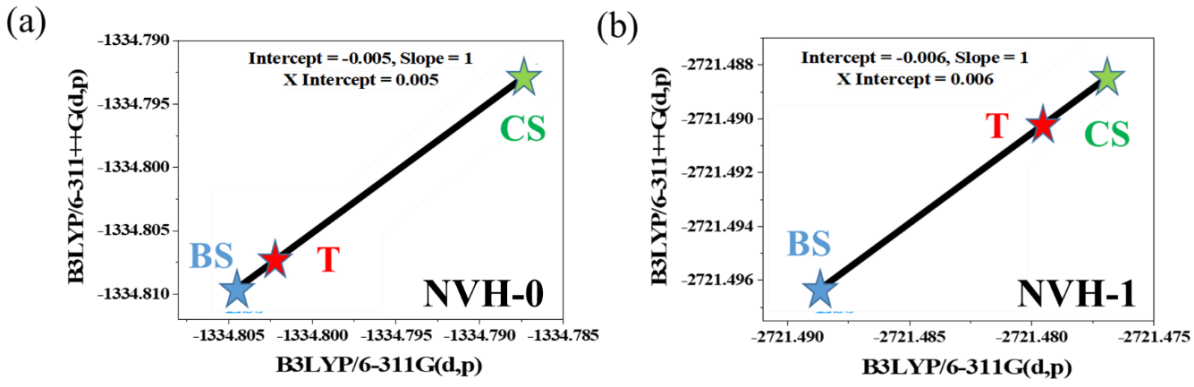

Figure S1. Energies (a.u.) of BS, T, and CS states of the initial state structure (a) NVH-0 and (b) NVH-1 at two calculation levels of the B3LYP/6-311G(d,p) and B3LYP/6-311++G(d,p).

2. Main Geometrical Parameters

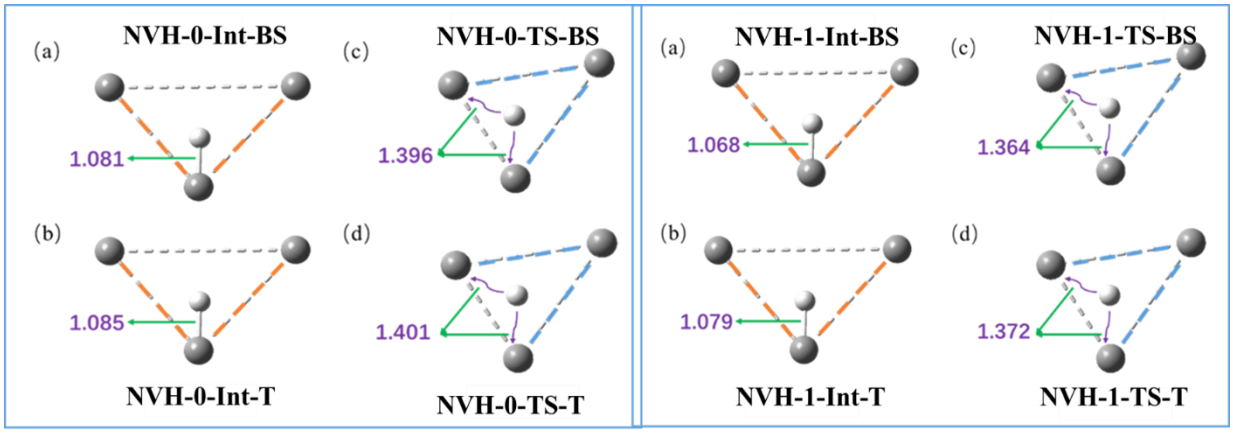

Figure S3. Distances between the H atom and C_1 and C_2 radicals of NVH-0 and NVH-1 in the Int and TS under BS or T states calculated at the B3LYP/6-311G(d,p) level.

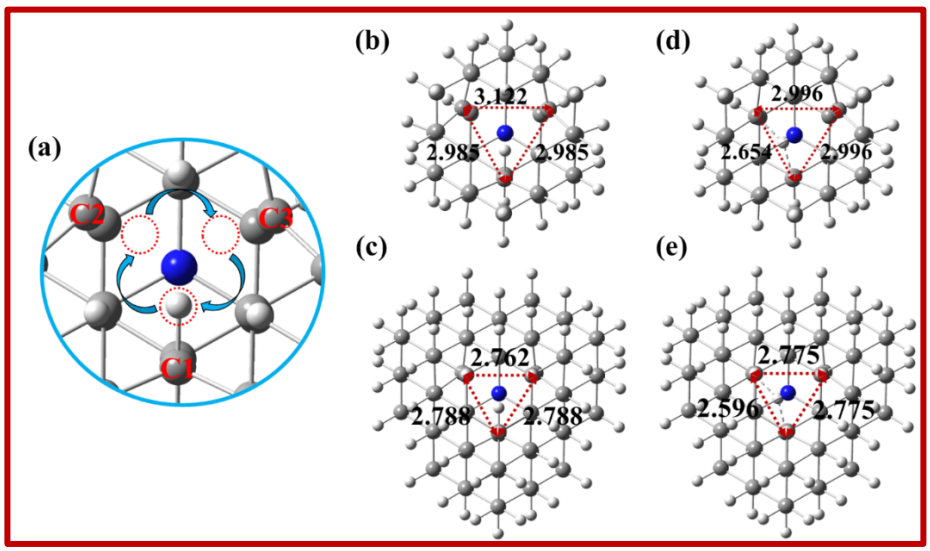

Figure 4(A). (a) The number of three C-radicals for the NVH center, and the distances between three C-radicals of **(b)** NVH-0 (Int), **(c)** NVH-1 (Int), **(d)** NVH-0 (TS), and **(e)** NVH-1 (TS), calculated at the B3LYP/6-311G(d,p) level.

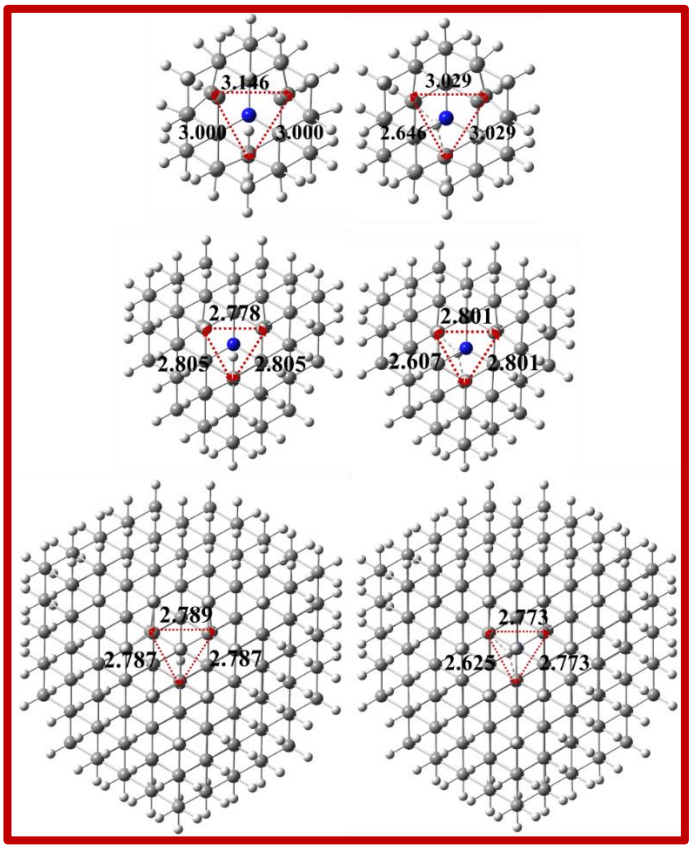

Figure S4(B). Distances between three C-radicals of NVH-0, NVH-1, and NVH-2, calculated at the B3LYP/6-311G(d,p) (three C, one N, and one H in the inner-sphere)||B3LYP/STO-3G (all C and H atoms in the outer-sphere) level.

3. All Calculated Energies

Table S1(A). Energies in the BS, T, CS, and Q states of NVH-0 and NVH-1 in the TS, calculated at the B3LYP/6-311G(d,p) level.

Diamond	E_{BS}/(a.u.)	E_{T}/(a.u.)	E_{CS}/(a.u.)	E_{Q}/(a.u.)
NVH-0	-1334.76926	-1334.77029	-1334.73116	-1334.70411
NVH-1	-2721.45844	-2721.46027	-2721.41325	-2721.34282

Table S1(B). Energies in the BS, T, and CS of NVH-0-Int and NVH-1-Int calculated at the B3LYP/6-311G(d,p) and B3LYP/6-311++G(d,p) levels and energies of NVH-2-Int in the BS, T, and CS calculated at the B3LYP/6-311G(d,p) (three C, one N, and one H in the inner-sphere)||B3LYP/STO-3G (all C and H atoms in the outer-sphere) level.

Diamond	Computational Level	E_{BS}/(a.u.)	E_T/(a.u.)	E_{CS}/(a.u.)
NVH-0	B3LYP/6-311G(d,p)	-1334.80379	-1334.80158	-1334.78737
	B3LYP/6-311++G(d,p)	-1334.80931	-1334.80711	-1334.79246
NVH-1	B3LYP/6-311G(d,p)	-2721.48776	-2721.48309	-2721.48334
	B3LYP/6-311++G(d,p)	-2721.49608	-2721.49142	-2721.48792
NVH-2	B3LYP/6-311G(d,p)||STO-3G	-10044.70748	-10044.70294	-10044.69319

Table S1(C). The energies of different multiple states of two sizes of the NVH center diamond, calculated at the B3LYP/6-311++G(d,p) level. [a]

B3LYP/6-311++G(d,p)		E_T/a.u. ($<S^2>$)	E_{BS}/a.u. ($<S^2>$)	E_{CS}/a.u. ($<S^2>$)	E_Q/a.u. ($<S^2>$)
NV-0-H	N-H:1.003 Å	-1334.72719 (2.025)	-1334.71658 (1.018)	-1334.68589 (0.000)	-1334.65177 (6.013)
	N-H:2.090 Å	-1334.73108 (2.046)	-1334.71617 (1.013)	-1334.68059 (0.000)	-1334.59694 (6.019)
NV-1-H	N-H:1.071 Å	-2721.42966 (2.015)	-2721.41791 (1.005)	-2721.38309 (0.000)	-2721.34128 (6.011)
	N-H:1.990 Å	-2721.44565 (2.021)	-2721.42922 (1.006)	-2721.39216 (0.000)	-2721.31723 (6.017)

[a]**Note:** The H atom is placed into the optimized NV centers, where the distances from the H atom to the N atom are divided into two categories, one is from the optimized structure that the H atom bonding with the N atom (1.003 Å for NV-0-H, and 1.071 Å for NV-1-H), and one is from the optimized structure NVH-0 and NVH-1 whose N-H distance are 2.090 Å and 1.990 Å, respectively. Results reveal that the stable state (T) energy of these four models is all higher than the structures that the H atom bonded with one of the C-radical.

Table S2. Energies in the BS and T states and energy gaps ($\Delta E_{(BS-T)}$, kcal·mol^{-1}) of NVH-0 and NVH-1 in the Int and TS, calculated at the B3LYP/6-311G(d,p), B3LYP/6-311++G(d,p) and CASSCF(4,3)-MP2/3-21G* levels.

Diamonds	Calculation Levels	E_{BS} (a.u.)	E_T (a.u.)	$\Delta E_{(BS-T)}$ (kcal·mol^{-1})
NVH-0-Int BS	B3LYP/6-311G(d,p)	-1334.80379	-1334.80158	-1.39
	B3LYP/6-311++G(d,p)	-1334.80931	-1334.80711	-1.38
	wB97XD/def2-TZVP	-1334.63717	-1334.63508	-1.31
	CASSCF(4,3)-MP2/3-21G*	-1321.47492	-1321.47757	-1.67
NVH-1-Int BS	B3LYP/6-311G(d,p)	-2721.48776	-2721.48309	-2.93
	B3LYP/6-311++G(d,p)	-2721.49608	-2721.49142	-2.93
	wB97XD/def2-TZVP	-2721.23612	-2721.23130	-3.02
	CASSCF(4,3)-MP2/3-21G*	-2702.17899	-2702.17403	-3.23

Table S3. Energies of SOMO-α1 and SOMO-α2 of NVH-0 and NVH-1 in the Int-T and TS-T.

	SOMO-α1 (a.u.)	SOMO-α2 (a.u.)	SOMO-SOMO (a.u.)	SOMO-SOMO (eV)
NVH-0-Int	-0.163	-0.150	0.014	0.376
NVH-1-Int	-0.150	-0.133	0.017	0.455
NVH-0-TS	-0.155	-0.150	0.006	0.159
NVH-1-TS	-0.140	-0.137	0.003	0.075

Table S4(A). The initial state energy (E_{Int}, a.u.), transition state energy (E_{TS}, a.u.), and activation energy (Ea, kcal·mol^{-1}) of NVH-0 and NVH-1 in BS state, calculated at the B3LYP/6-311G (d,p) and B3LYP/6-311++G (d,p) levels.

		Broken-Symmetry Open-Shell Singlet		
Diamond	**Basis Set**	**E_{Int}/a.u.**	**E_{TS}/a.u.**	**Ea/kcal·mol^{-1}**
NVH-0	6-311G(d,p)	-1334.80379	-1334.76926	22.00
	6-311++G(d,p)	-1334.80931	-1334.73762	25.10
NVH-1	6-311G(d,p)	-2721.48776	-2721.45844	18.40
	6-311++G(d,p)	-2721.49608	-2721.46676	18.40

Table S4(B). The initial state energy (E_{Int}, a.u.), transition state energy (E_{TS}, a.u.), and activation energy (Ea, kcal·mol^{-1}) of NVH-0 and NVH-1 in T, calculated at the B3LYP/6-311G (d,p) and B3LYP/6-311++G (d,p) levels.

		Broken-Symmetry Open-Shell Triplet		
Diamond	**Basis Set**	**E_{Int}/a.u.**	**E_{TS}/a.u.**	**Ea/kcal·mol^{-1}**
NVH-0	6-311G(d,p)	-1334.80158	-1334.77009	20.14
	6-311++G(d,p)	-1334.80711	-1334.77570	23.22
NVH-1	6-311G(d,p)	-2721.48309	-2721.46027	14.32
	6-311++G(d,p)	-2721.49142	-2721.46858	14.33

Table S4(C). The following Ea was calculated with the stable state of Int and TS, that is **Ea=E_T (TS)-E_{BS} (Int)**, calculated at the B3LYP/6-311G (d,p) and B3LYP/6-311++G (d,p) levels.

Diamond	**Basis Set**	**E_{Int}/a.u.**	**E_{TS}/a.u.**	**Ea/ kcal·mol^{-1}**
NVH-0	6-311G(d,p)	-1334.80379	-1334.77009	21.02
	6-311++G(d,p)	-1334.80931	-1334.77570	20.98
NVH-1	6-311G(d,p)	-2721.48776	-2721.46027	17.25
	6-311++G(d,p)	-2721.49608	-2721.46858	17.25

Table S4(D). The initial state energy (E_{Int}, a.u.), transition state energy (E_{TS}, a.u.), and activation energy (Ea, kcal·mol^{-1}) of NVH-0, NVH-1, and NVH-2 in BS, calculated at the B3LYP/6-311G(d,p) (three C, one N, and one H in the inner-sphere)||B3LYP/STO-3G (all C and H atoms in the outer-sphere) level.

	Broken-Symmetry Open-Shell Singlet		
Diamond	**E_{Int}/a.u.**	**E_{TS}/a.u.**	**Ea/kcal·mol^{-1}**
NVH-0	-1320.76834	-1320.73205	22.59
NVH-1	-2690.82188	-2690.79077	19.80
NVH-2	-10044.70748	-10044.67585	19.91

Table S4(E). The initial state energy (E_{Int}, a.u.), transition state energy (E_{TS}, a.u.), and activation energy (Ea, kcal·mol^{-1}) of NVH-0, NVH-1 and NVH-2 in T, calculated at the B3LYP/6-311G(d,p) (three C, one N, and one H in the inner-sphere)||B3LYP/STO-3G (all C and H atoms in the outer-sphere) level.

	Broken-Symmetry Open-Shell Triplet		
Diamond	**E_{Int}/a.u.**	**E_{TS}/a.u.**	**Ea/kcal·mol^{-1}**
NVH-0	-1320.76636	-1320.73308	21.04
NVH-1	-2690.81718	-2690.79265	15.35
NVH-2	-10044.70294	-10044.67783	15.81

Table S4(F). The following Ea was calculated with the stable state of Int and TS, that is **Ea=E_T (TS)-E_{BS} (Int)**, calculated at the B3LYP/6-311G(d,p) (three C, one N, and one H in the inner-sphere)||B3LYP/STO-3G (all C and H atoms in the outer-sphere) level.

Diamond	**E_{Int}/a.u.**	**E_{TS}/a.u.**	**Ea/kcal·mol^{-1}**
NVH-0	-1320.76834	-1320.73308	22.13
NVH-1	-2690.82188	-2690.79265	18.34
NVH-2	-10044.70748	-10044.67783	18.61

4. The Corresponding Magnetic *J* Spin Coupling Constants

Table S5. Energies and $<S^2>$ values of BS and T states, and magnetic exchange coupling constants (J, cm^{-1}) of NVH-0 and NVH-1 in the Int and TS, calculated at the wB97XD/def2-TZVP, B3LYP/6-311G(d,p), and B3LYP/6-311++G(d,p)) levels.

Diamond	Computational Level	E_{BS} /a.u. ($<S^2>$)	E_T /a.u. ($<S^2>$)	J/(cm^{-1})
NVH-0-Int	wB97XD/def2-TZVP	-1334.63717 (0.972)	-1334.63508 (2.011)	-416.26
	B3LYP/6-311G(d,p)	-1334.80379 (0.950)	-1334.80158 (2.009)	-458.23
	B3LYP/6-311++G(d,p)	-1334.80931 (0.950)	-1334.80711 (2.009)	-455.52
NVH-1-Int	wB97XD/def2-TZVP	-2721.23612 (0.872)	-2721.23130 (2.010)	-964.28
	B3LYP/6-311G(d,p)	-2721.48776 (0.854)	-2721.48309 (2.008)	-887.61
	B3LYP/6-311++G(d,p)	-2721.49608 (0.854)	-2721.49142 (2.008)	-886.27
NVH-0-TS	wB97XD/def2-TZVP	-1334.60219 (1.015)	-1334.60325 (2.015)	219.47
	B3LYP/6-311G(d,p)	-1334.76926 (1.012)	-1334.77029 (2.012)	227.24
	B3LYP/6-311++G(d,p)	-1334.76926 (1.012)	-1334.77028 (2.012)	224.08
NVH-1-TS	wB97XD/def2-TZVP	-2721.20539 (1.016)	-2721.20732 (2.014)	439.82
	B3LYP/6-311G(d,p)	-2721.45844 (1.010)	-2721.46027 (2.011)	401.03
	B3LYP/6-311++G(d,p)	-2721.46676 (1.011)	-2721.46858 (2.011)	399.39

Table S6. Energies and $<S^2>$ values of BS and T states, and magnetic exchange coupling constants (J, cm^{-1}) of NVH-0, NVH-1, and NVH-2 in the Int and TS, calculated at the B3LYP/6-311G(d,p) (three C, one N, and one H in the inner-sphere)||B3LYP/STO-3G (all C and H atoms in the outer-sphere) level.

		B3LYP/6-311G(d,p)||B3LYP/STO-3G				
		E_{BS} /(a.u.)	$<S^2>_{BS}$	E_T/(a.u.)	$<S^2>_T$	J/(cm^{-1})
Int	NVH-0	-1320.76834	0.963	-1320.76636	2.009	-414.53
	NVH-1	-2690.82188	0.867	-2690.81718	2.007	-903.78
	NVH-2	-10044.70748	0.879	- 10044.70294	2.007	-883.40
TS	NVH-0	-1320.73205	1.012	-1320.73308	2.013	226.80
	NVH-1	-2690.79077	1.010	-2690.79265	2.011	411.74
	NVH-2	-10044.67585	1.010	-10044.67783	2.011	434.11

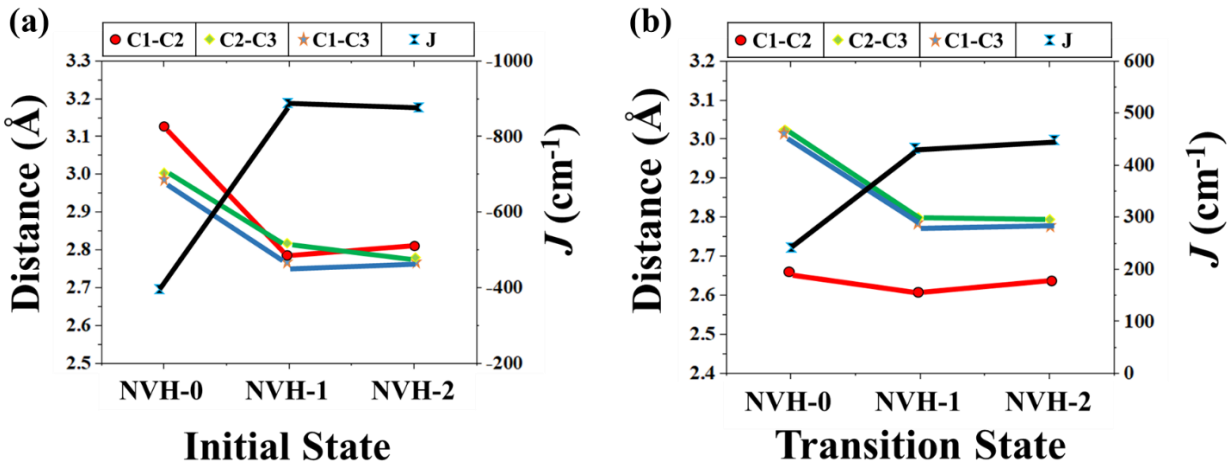

Figure S5. Under the calculation of B3LYP/6-311G(d,p) (three C, one N, and one H in the inner-sphere)||B3LYP/STO-3G (all C and H atoms in the outer-sphere) level, the relationship between the magnetic coupling constants and distances of three C-radicals of the NVH-0, NVH-1, and NVH-2 in the (a) Int and (b) TS.

5. Orbital Information and Spin Density

Table S7. The magnetic moments (in μB, the Bohr magneton) of an α-spin electron distributed on three C-radicals and H radical (β takes the opposite value) of the NVH-0 and NVH-1 in the Int and TS.

	NVH-0	**Magnetic Moment (μB)**		**NVH-1**	**Magnetic Moment (μB)**	
Type	**Atom**	**Int**	**TS**	**Atom**	**Int**	**TS**
s	N	0.000	-0.000	N	-0.000	-0.000
p		0.001	0.001		0.001	0.001
d		0.000	0.000		0.000	0.000
s	C_1	0.000	0.067	C_1	0.000	0.068
p		0.000	0.433		0.000	0.439
d		0.000	-0.000		0.000	0.000
s	C_2	0.083	0.067	C_2	-0.091	0.068
p		0.829	0.433		-0.791	0.439
d		-0.001	0.000		0.002	0.000
s	C_3	-0.083	0.079	C_3	0.091	0.090
p		-0.829	0.855		0.791	0.848
d		0.001	-0.001		-0.002	-0.001
s	H	0.000	-0.084	H	0.000	-0.082
p		0.000	0.017		0.000	0.019
Total		~0	~1		~0	~1

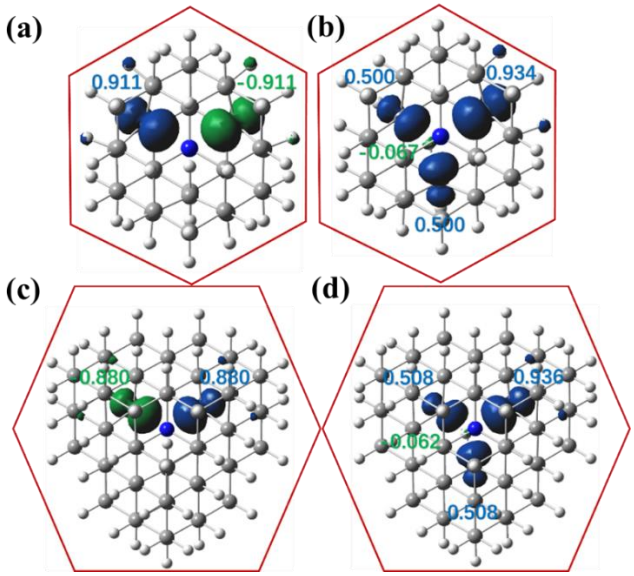

Figure S6. Spin density distributions (isovalue=0.01) of the (a) NVH-0-Int, (b) NVH-0-TS, (c) NVH-1-Int, and (d) NVH-1-TS.

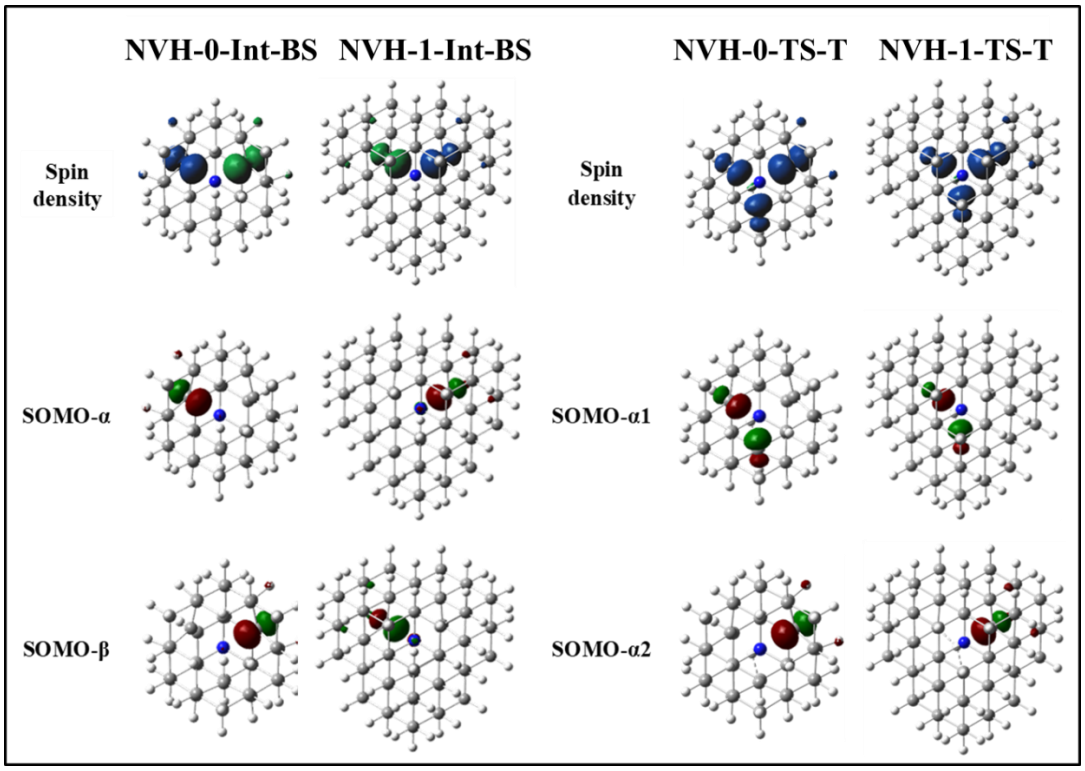

Figure S7. The spin density distributions (isovalue=0.01) and singly occupied molecular orbitals (SOMOs) (isovalue=0.1) for the optimized structures of the NVH-0 and NVH-1 at the Int and TS.

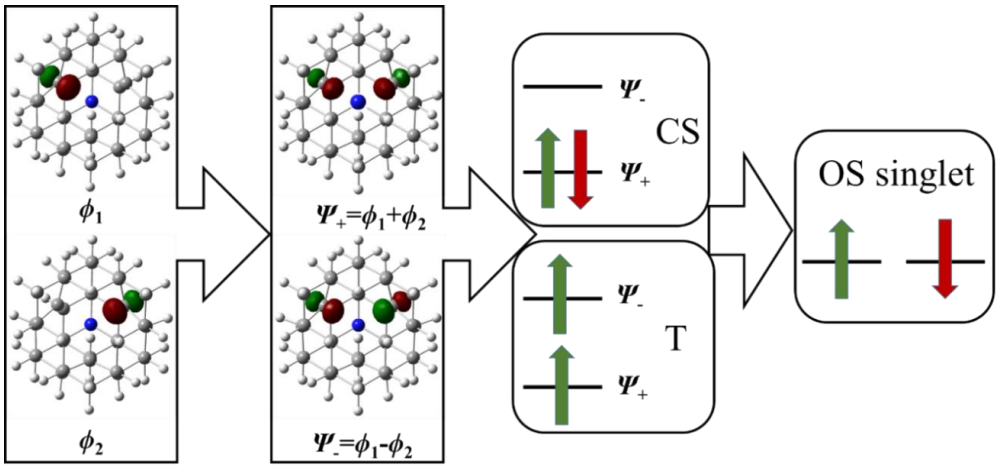

Figure S8. Molecular orbital interactions and electronic state coupling mechanism of the initial state structure, calculated at the B3LYP/6-311G(d,p) level.

6. Dynamic Magnetic Characterization along the IRC Path

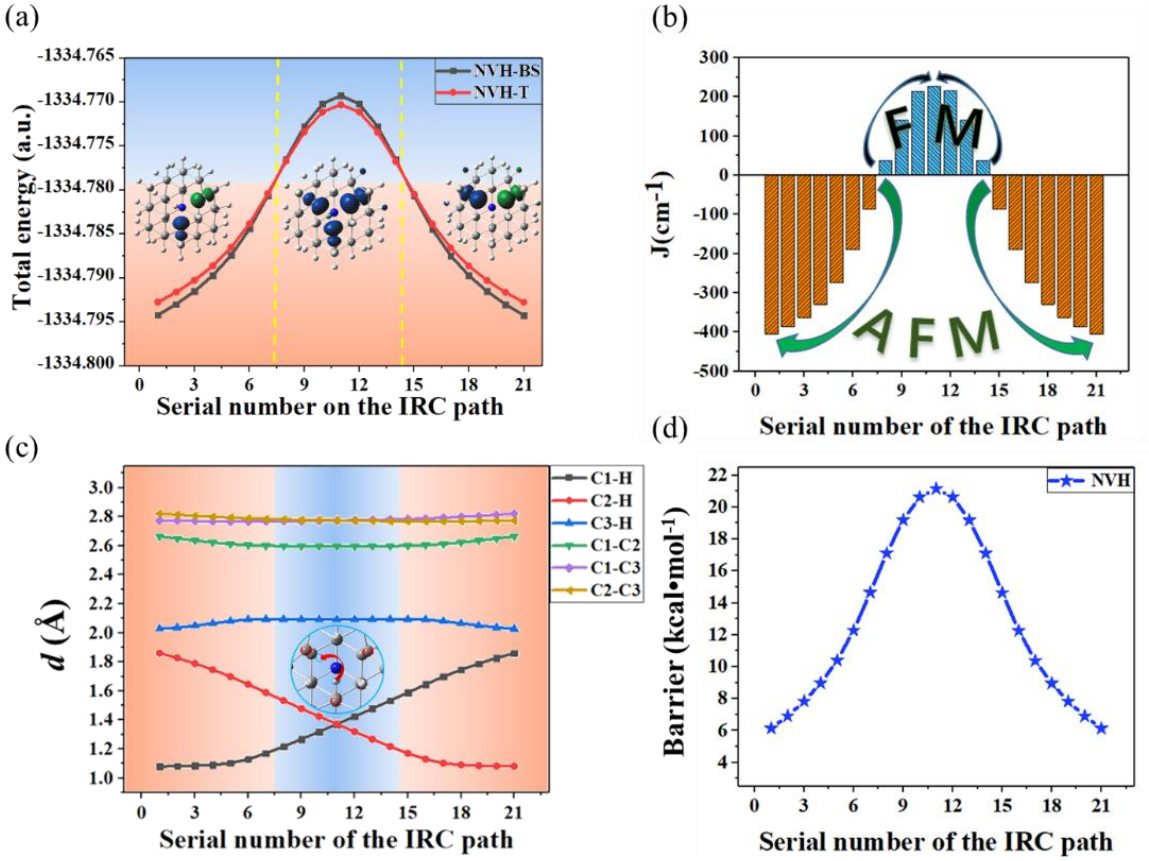

Figure S9(A). (a) Total energies along the IRC-BS and IRC-T paths of the NVH-0. (b) The magnetic exchange coupling constants (J/cm^{-1}) along the IRC. (c) Distances (Å) of the C-C and C-H along the IRC path. (d) Energy barriers (kcal·mol^{-1}) along the IRC path.

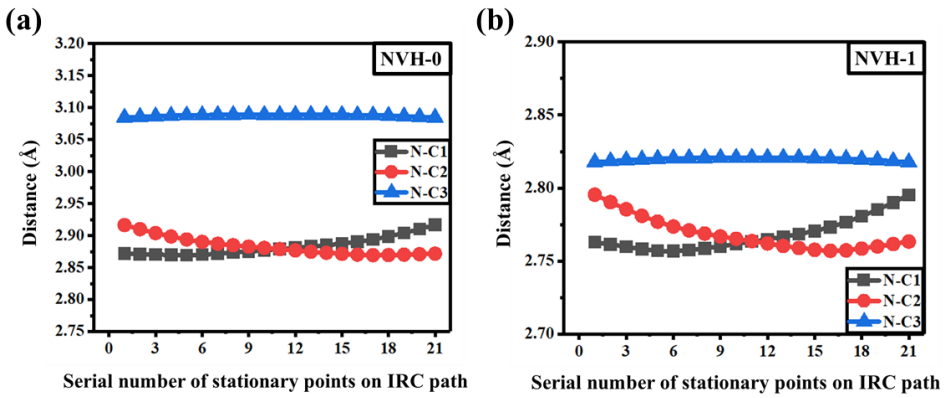

Figure S9(B). The distances (Å) of the N-H and N-C when the H migrates from the C_1-atom to C_2-radical along the IRC path of the (a) NVH-0 and (b) NVH-1.

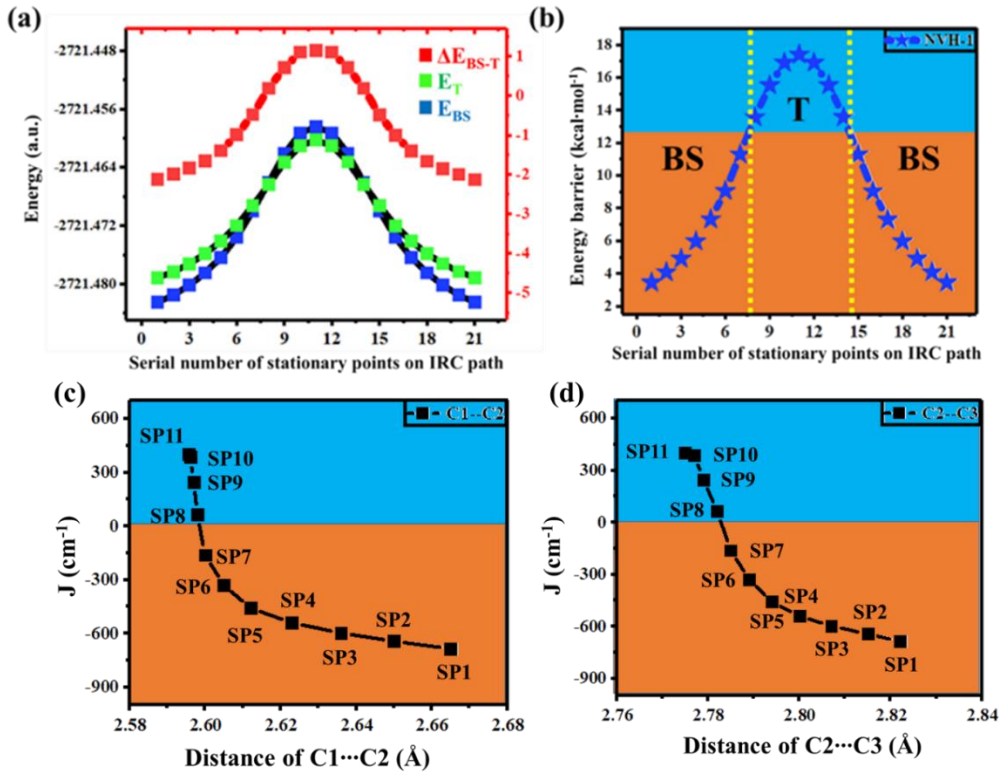

Figure S10. (a) The single point energies of the BS and T states (SP1-7 and SP15-21 are calculated by taking the covalent BS stationary points of SP1-7 and SP15-21, and SP8-14 are calculated by taking the covalent T stationary points of SP8-14) and the energy difference, ΔE_{BS-T} along the IRC path. (b) Energy barriers (kcal·mol^{-1}) between the stationary structures at ground state (SP1-7 and SP15-21 are BS, and SP8-14 are T state) and TS in T state along the IRC path. (c) The relationship between *J* and distances of $C_1 \cdots C_2$ and (d) $C_2 \cdots C_3$ of the NVH-1, calculated at the B3LYP/6-311G(d,p) level.

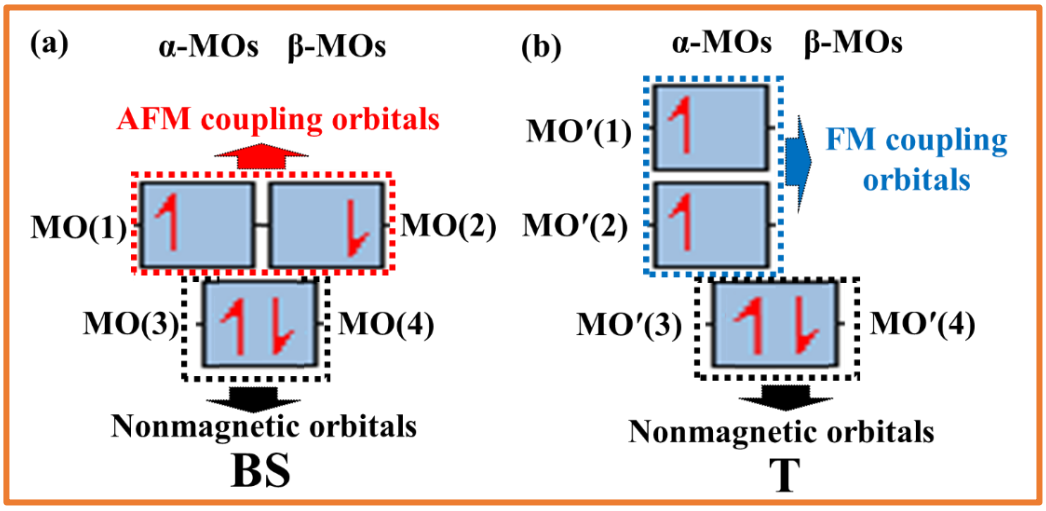

Figure S11(A). During the MO evolution, the change in the relative position of the energy level between the α- and β-orbitals for magnetic coupling of the NVH center, which is from the BS initial state to T-TS, leading to the switching of the AFM and FM coupling. MO(1-2) and MO′(1-2) orbitals represent the highest occupied MOs corresponding to magnetic spin coupling. MO(3-4) and MO′(3-4) orbitals are corresponding to the bonding orbitals of C_1-H. It is important to note that here the MO(1-4) and MO′(1-4) orbitals are not directly transformed, but are gradually recombined during orbitals evolution. In this evolutionary process, orbitals have mixing and electrons have leaps or spin reversals. However, the abstract evolutionary process is neglected in order to show directly and clearly the orbital distribution results of the initial state and TS. **Note: the next MO(1) and MO (2) are associated with ψ_a and ψ_b, and MO(3) and MO (4) are associated with ψ_c in the paper.**

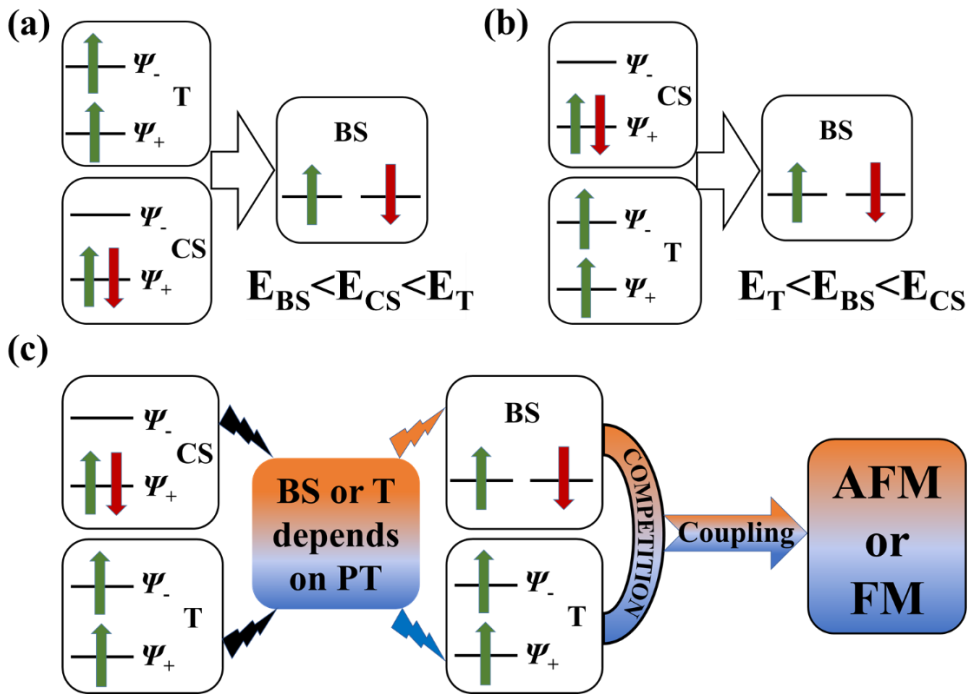

Figure S11(B). The BS state is obtained due to interaction between the CS and T states. **(a)** In the case of the CS state lower than the T state, the resulting BS state generally becomes the ground state. **(b)** In the case of the CS state higher than the T state, the resulting BS state is generally in the order of $E_T < E_{BS} < E_{CS}$ and the T state is still the ground state. **(c)** Molecular orbital interactions and electronic state coupling mechanism for AFM or FM.

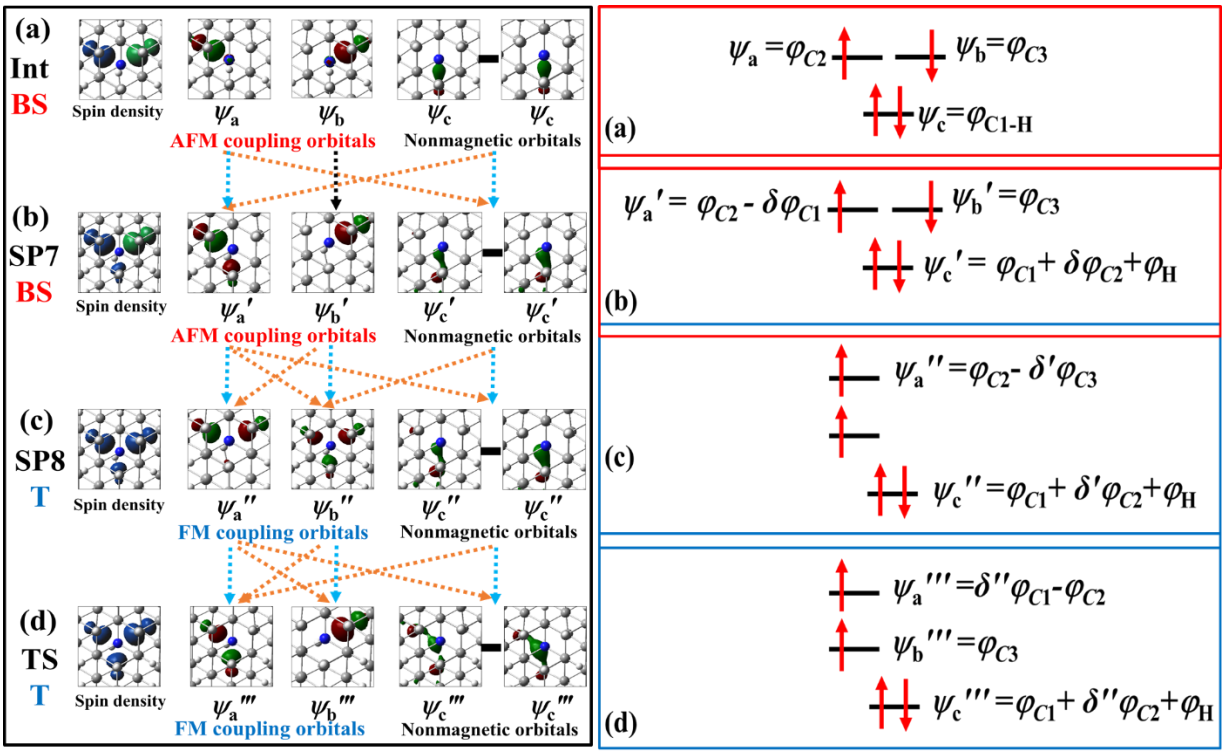

Figure S11(C). Left panel) Spin density distribution (isovalue = 0.01) and two singly occupied MOs (isovalue = 0.1) associated with magnetic spin coupling and low-energy bonding MO of C_1-H of NVH-1 at the **Int** state **(a)** and three representative configurations (**(b)** SP7, **(c)** SP8, **(d)** SP11(TS)) on the IRC path, calculated at the B3LYP/6-311G(d,p) level. The black arrow is referred to the unchanging in the MO distribution on some C, and the orange arrow is referred to the increase in the MO distribution on some C, while the blue arrow is referred to the decrease in the MO distribution on some C. **Right panel)** During the MO evolution, the relative position of the energy level among magnetic coupling orbitals and nonmagnetic orbitals, and the MOs composition of the **Ini** state **(a)** and three representative configurations (**(b)** SP7, **(c)** SP8, and **(d)** SP11(TS)) on the IRC path of NVH-1. In this evolutionary process, molecular orbitals are mixed and spin flip of an electron takes place, leading to the electronic state (BS) transition to the T state.

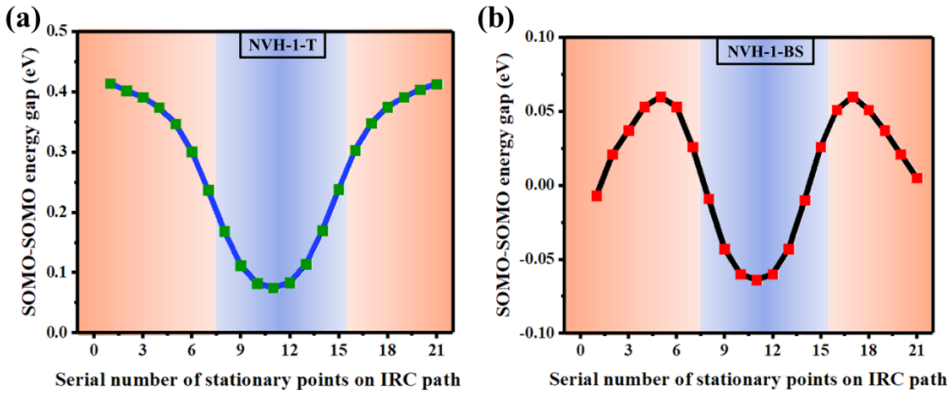

Figure S11(D). The energy gaps of two SOMOs in the T and BS changing along the IRC path of the NVH-1, calculated at the B3LYP/6-311G(d,p) level.

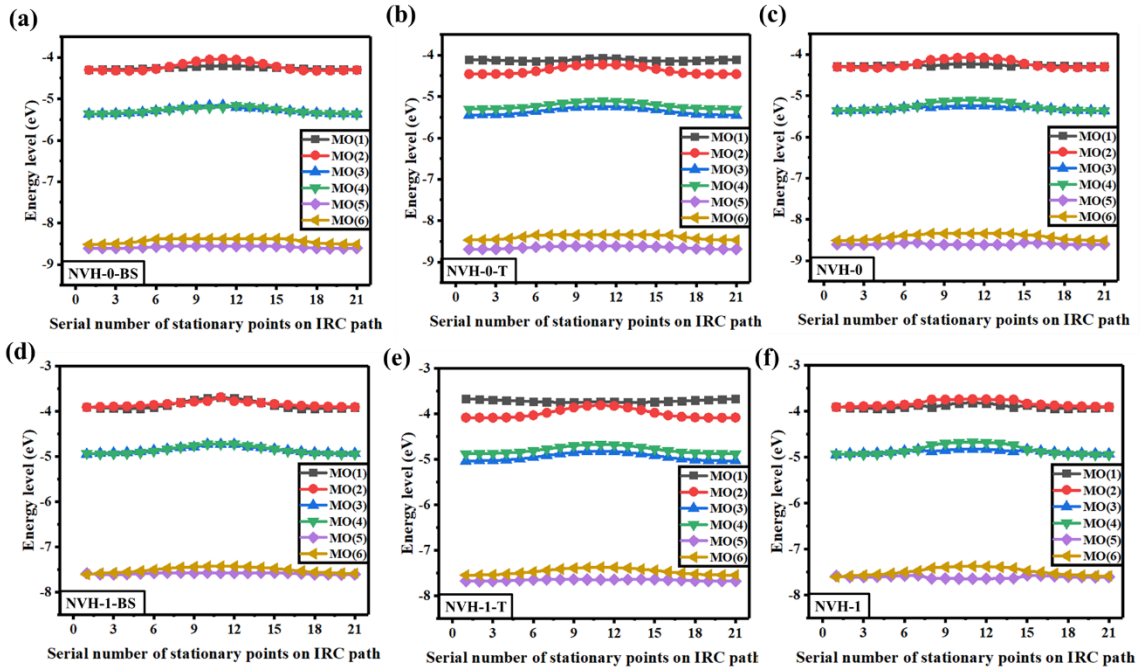

Figure S11(E). (a)-(b) The energy levels of MO(1)-MO(6) along the IRC path of the NVH-0 in the BS and T states, respectively. (c) The energy levels of MO(1)-MO(6) in the minima energy path (the energy stationary points 1 to 7 and points 15 to 21 is BS/ the energy stationary points 8 to 14 is T) of NVH-0 along the IRC. (d)-(e) The energy levels of MO(1)-MO(6) along the IRC path of the NVH-1 in BS and T states, respectively. (f) The energy levels of MO(1)-MO(6) in the minima energy path (the energy SP1 to 7 and SP15 to 21 is BS/ the energy SP8 to 14 is T) of NVH-1 along the IRC path. MO(1-2) orbitals represent the highest occupied MOs corresponding to magnetic spin coupling. MO(3-4) orbitals are corresponding to the bonding orbitals of C_1-H. MO(5-6) orbitals are corresponding to the orbitals of two lone pair of electron orbitals on N.

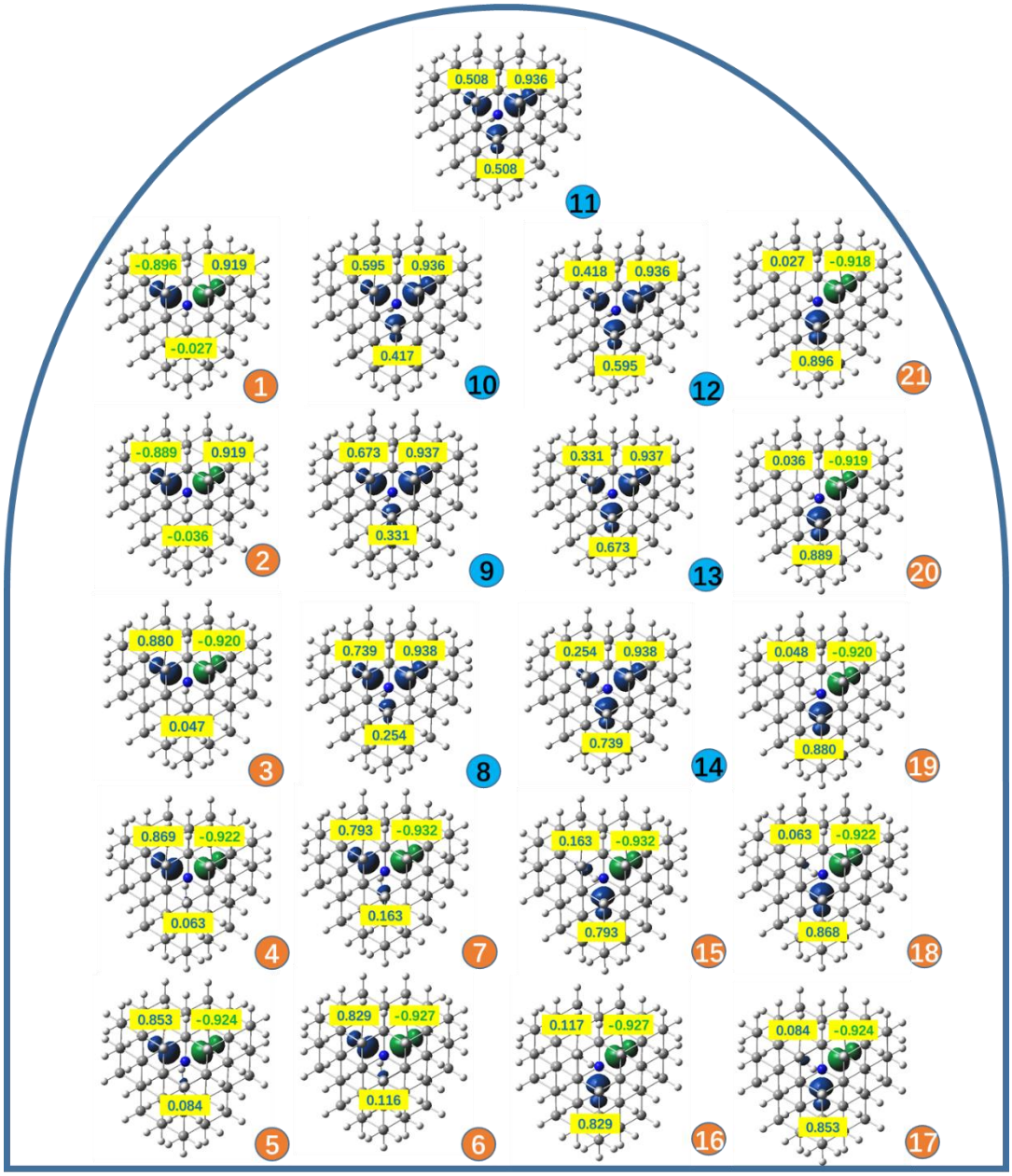

Figure S12. Spin density distributions (isovalue=0.01) of the NVH-1 along the IRC path.

Table S8(A). The distances (Å) of C-C and C-H, and angles (°) of ∠C_1-H-C_2 and ∠ H-C_1-C_2 along the IRC path of the NVH-0, calculated at the B3LYP/6-311G(d,p) level.

IRC	C_1-H	C_2-H	C_3-H	C_1-C_2	C_1-C_3	C_2-C_3	∠C_1-H-C_2	∠H-C_1-C_2
Initial	1.081	2.220	2.220	2.985	2.985	3.122	125.9	37.1
1	1.090	1.891	2.271	2.717	2.989	3.043	129.8	32.3
2	1.091	1.858	2.280	2.702	2.988	3.035	131.4	31.1
3	1.094	1.821	2.294	2.688	2.987	3.027	133.5	29.4
4	1.101	1.778	2.309	2.676	2.986	3.020	136.1	27.5
5	1.119	1.729	2.323	2.667	2.986	3.014	138.6	25.4
6	1.153	1.674	2.331	2.660	2.987	3.010	140.6	23.5
7	1.197	1.618	2.332	2.657	2.988	3.006	141.8	22.1
8	1.245	1.563	2.332	2.655	2.990	3.003	142.6	21.4
9	1.296	1.508	2.330	2.654	2.992	3.001	143.2	20.4
10	1.349	1.455	2.329	2.654	2.994	2.998	143.4	19.5
11	1.401	1.401	2.328	2.654	2.996	2.996	143.5	18.8
12	1.455	1.349	2.328	2.654	2.999	2.994	143.4	18.1
13	1.509	1.297	2.330	2.654	3.001	2.992	143.2	17.5
14	1.563	1.246	2.331	2.655	3.003	2.990	142.5	16.9
15	1.618	1.197	2.332	2.657	3.006	2.988	141.7	16.1
16	1.674	1.153	2.330	2.660	3.010	2.987	140.5	15.9
17	1.729	1.119	2.323	2.667	3.015	2.986	138.6	16.0
18	1.779	1.101	2.309	2.676	3.021	2.986	136.0	16.5
19	1.821	1.094	2.294	2.688	3.028	2.987	133.5	17.1
20	1.859	1.091	2.280	2.702	3.035	2.987	131.4	17.5
21	1.891	1.089	2.270	2.717	3.044	2.988	129.8	17.9

Table S8(B). The distances (Å) of C-C and C-H, and angles (°) of ∠C_1-H-C_2 and ∠H-C_1-C_2 along the IRC path of the NVH-1, calculated at the B3LYP/6-311G(d,p) level.

IRC	C_1-H	C_2-H	C_3-H	C_1- C_2	C_1-C_3	C_2-C_3	∠C_1-H-C_2	∠H-C_1-C_2
Initial	1.068	2.020	2.017	2.788	2.788	2.762	126.3	35.7
1	1.080	1.861	2.029	2.665	2.773	2.822	128.6	33.0
2	1.083	1.828	2.037	2.650	2.771	2.815	130.3	31.7
3	1.086	1.789	2.050	2.636	2.770	2.807	132.6	29.9
4	1.091	1.747	2.066	2.623	2.768	2.800	135.2	27.9
5	1.103	1.699	2.081	2.612	2.767	2.794	138.0	25.7
6	1.130	1.646	2.092	2.605	2.766	2.789	140.3	23.7
7	1.171	1.589	2.095	2.600	2.767	2.785	141.9	22.1
8	1.218	1.534	2.095	2.598	2.769	2.782	142.8	21.7
9	1.268	1.479	2.094	2.597	2.770	2.779	143.4	20.6
10	1.319	1.425	2.093	2.596	2.772	2.777	143.5	19.7
11	1.372	1.372	2.093	2.596	2.775	2.775	143.6	18.9
12	1.425	1.320	2.093	2.596	2.776	2.773	143.5	18.2
13	1.479	1.268	2.094	2.597	2.779	2.771	143.4	17.6
14	1.534	1.218	2.095	2.598	2.781	2.769	142.8	17.1
15	1.589	1.171	2.095	2.600	2.784	2.768	141.9	16.0
16	1.645	1.130	2.092	2.605	2.788	2.767	140.3	16.0
17	1.699	1.103	2.081	2.612	2.793	2.767	138.0	16.3
18	1.746	1.091	2.066	2.623	2.800	2.768	135.2	16.9
19	1.789	1.086	2.051	2.636	2.807	2.770	132.6	17.5
20	1.828	1.083	2.038	2.650	2.814	2.772	130.3	18.0
21	1.860	1.082	2.028	2.665	2.822	2.773	128.6	18.3

Table S8(C). The average distances (Å) of C_1-C_2, C_1-C_3, and C_2-C_3 along the IRC path of the NVH-0 and NVH-1, calculated at the B3LYP/6-311G(d,p) level.

	NVH-0				NVH-1			
IRC	**C_1-C_2**	**C_1-C_3**	**C_2-C_3**	**Average**	**C_1-C_2**	**C_1-C_3**	**C_2-C_3**	**Average**
Initial	2.985	2.985	3.122	3.031	2.788	2.788	2.762	2.779
1	2.717	2.989	3.043	2.916	2.665	2.773	2.822	2.753
2	2.702	2.988	3.035	2.908	2.650	2.771	2.815	2.745
3	2.688	2.987	3.027	2.901	2.636	2.770	2.807	2.738
4	2.676	2.986	3.020	2.894	2.623	2.768	2.800	2.730
5	2.667	2.986	3.014	2.889	2.612	2.767	2.794	2.724
6	2.660	2.987	3.010	2.886	2.605	2.766	2.789	2.720
7	2.657	2.988	3.006	2.884	2.600	2.767	2.785	2.717
8	2.655	2.990	3.003	2.883	2.598	2.769	2.782	2.716
9	2.654	2.992	3.001	2.882	2.597	2.770	2.779	2.715
10	2.654	2.994	2.998	2.882	2.596	2.772	2.777	2.715
11	2.654	2.996	2.996	2.882	2.596	2.775	2.775	2.715
12	2.654	2.999	2.994	2.882	2.596	2.776	2.773	2.715
13	2.654	3.001	2.992	2.882	2.597	2.779	2.771	2.716
14	2.655	3.003	2.990	2.883	2.598	2.781	2.769	2.716
15	2.657	3.006	2.988	2.884	2.600	2.784	2.768	2.717
16	2.660	3.010	2.987	2.886	2.605	2.788	2.767	2.720
17	2.667	3.015	2.986	2.889	2.612	2.793	2.767	2.724
18	2.676	3.021	2.986	2.894	2.623	2.800	2.768	2.730
19	2.688	3.028	2.987	2.901	2.636	2.807	2.770	2.738
20	2.702	3.035	2.987	2.908	2.650	2.814	2.772	2.745
21	2.717	3.044	2.988	2.916	2.665	2.822	2.773	2.753

Table S8(D). The distances (Å) of N-H and N-C along the IRC path of the NVH-0 and NVH-1, calculated at the B3LYP/6-311G(d,p) level.

	NVH-0				NVH-1			
IRC	**N-H**	**N-C_1**	**N- C_2**	**N-C_3**	**N-H**	**N-C_1**	**N- C_2**	**N-C_3**
Initial	2.090	2.868	3.012	3.012	1.990	2.770	2.806	2.805
1	2.149	2.872	2.916	3.085	2.027	2.763	2.795	2.818
2	2.161	2.871	2.910	3.086	2.039	2.761	2.790	2.818
3	2.177	2.870	2.904	3.087	2.055	2.760	2.785	2.819
4	2.194	2.870	2.898	3.087	2.074	2.758	2.781	2.820
5	2.210	2.870	2.894	3.088	2.092	2.757	2.777	2.820
6	2.218	2.870	2.890	3.088	2.104	2.757	2.774	2.820
7	2.220	2.872	2.887	3.089	2.109	2.757	2.771	2.820
8	2.220	2.873	2.885	3.089	2.110	2.759	2.769	2.821
9	2.219	2.875	2.883	3.089	2.109	2.760	2.767	2.821
10	2.217	2.877	2.881	3.089	2.108	2.762	2.765	2.821
11,TS	2.217	2.879	2.879	3.089	2.108	2.763	2.764	2.821
12	2.217	2.881	2.877	3.089	2.108	2.765	2.762	2.821
13	2.218	2.883	2.875	3.089	2.109	2.767	2.760	2.821
14	2.219	2.885	2.873	3.089	2.110	2.768	2.759	2.821
15	2.220	2.887	2.871	3.089	2.109	2.771	2.758	2.821
16	2.218	2.890	2.870	3.088	2.104	2.773	2.757	2.820
17	2.209	2.894	2.869	3.088	2.092	2.777	2.757	2.820
18	2.194	2.899	2.869	3.087	2.074	2.781	2.759	2.820
19	2.177	2.904	2.870	3.087	2.055	2.785	2.760	2.819
20	2.161	2.910	2.871	3.086	2.039	2.790	2.762	2.818
21	2.149	2.917	2.872	3.085	2.026	2.795	2.763	2.818

Table S9(A). The single point energies (the energy stable state of SP1 to SP7 and SP15 to SP21 is the BS state/the energy stable state of SP8 to SP14 is the T state), corresponding magnetic exchange coupling constants (J/cm^{-1}), and energy difference (ΔE_{BS-T}, kcal·mol^{-1}) of NVH-0 along the IRC path, calculated at the B3LYP/6-311G(d,p) level.

IRC	E_T	$<S^2>_T$	E_{BS}	$<S^2>_{BS}$	$\Delta E_{(BS-T)}$	J(cm^{-1})
1	-1334.79228	2.009	-1334.79422	0.962	-1.2173684	-405.32
2	-1334.79114	2.009	-1334.79298	0.963	-1.1546174	-387.10
3	-1334.78978	2.009	-1334.79151	0.965	-1.0855914	-363.27
4	-1334.78814	2.009	-1334.78970	0.968	-0.9789148	-329.39
5	-1334.78614	2.009	-1334.78743	0.972	-0.8094872	-273.95
6	-1334.78354	2.009	-1334.78443	0.979	-0.5584834	-189.41
7	-1334.78023	2.009	-1334.78064	0.987	-0.2572789	-86.58
8	-1334.77672	2.010	-1334.77655	0.996	0.1066766	37.45
9	-1334.77341	2.011	-1334.77277	1.004	0.4016061	140.04
10	-1334.77112	2.012	-1334.77014	1.010	0.6149593	214.52
11	-1334.77029	2.012	-1334.76926	1.012	0.6463348	227.24
12	-1334.77112	2.012	-1334.77014	1.010	0.6149593	215.01
13	-1334.77343	2.011	-1334.77278	1.004	0.4078812	140.81
14	-1334.77675	2.010	-1334.77657	0.996	0.1129517	38.23
15	-1334.78028	2.009	-1334.78068	0.987	-0.2510038	-85.98
16	-1334.78359	2.009	-1334.78447	0.979	-0.5522083	-189.08
17	-1334.78617	2.009	-1334.78747	0.972	-0.8157623	-273.79
18	-1334.78817	2.009	-1334.78973	0.968	-0.9789148	-329.13
19	-1334.78980	2.009	-1334.79153	0.965	-1.0855914	-362.88
20	-1334.79116	2.009	-1334.79300	0.963	-1.1546174	-386.63
21	-1334.79230	2.009	-1334.79423	0.962	-1.2110933	-405.35

Table S9(B). The single point energies (the energy stable state of SP1 to SP7 and SP15 to SP21 is the BS state/the energy stable state of SP8 to SP14 is the T state), corresponding magnetic exchange coupling constants (J/cm^{-1}), and energy difference (ΔE_{BS-T}, kcal·mol^{-1}) of NVH-1 along the IRC path, calculated at the B3LYP/6-311G(d,p) level.

IRC	E_T	$<S^2>_T$	E_{BS}	$<S^2>_{BS}$	$\Delta E_{(BS-T)}$	J(cm^{-1})
1	-2721.47913	2.008	-2721.48251	0.924	-2.1209820	-684.90
2	-2721.47832	2.008	-2721.48149	0.928	-1.9892050	-643.10
3	-2721.47724	2.008	-2721.48017	0.932	-1.8386027	-597.04
4	-2721.47584	2.008	-2721.47848	0.937	-1.6566250	-539.79
5	-2721.47412	2.008	-2721.47634	0.944	-1.3930710	-457.18
6	-2721.47199	2.008	-2721.47357	0.955	-0.9914650	-328.89
7	-2721.46924	2.008	-2721.47000	0.968	-0.4769072	-161.02
8	-2721.46638	2.009	-2721.46608	0.983	0.1882528	65.22
9	-2721.46327	2.010	-2721.46213	0.996	0.7153608	247.54
10	-2721.46107	2.010	-2721.45931	1.007	1.1044167	384.68
11	-2721.46027	2.011	-2721.45844	1.010	1.1483423	401.03
12	-2721.46106	2.010	-2721.45930	1.007	1.1044167	384.21
13	-2721.46325	2.010	-2721.46212	0.996	0.7090857	246.69
14	-2721.46636	2.009	-2721.46606	0.983	0.1882528	63.97
15	-2721.46925	2.008	-2721.47002	0.968	-0.4831823	-164.07
16	-2721.47201	2.008	-2721.47361	0.954	-1.0040152	-332.18
17	-2721.47413	2.008	-2721.47637	0.944	-1.4056212	-460.56
18	-2721.47584	2.008	-2721.47849	0.937	-1.6629001	-543.20
19	-2721.47723	2.008	-2721.48018	0.932	-1.8511529	-600.71
20	-2721.47831	2.008	-2721.48149	0.928	-1.9954801	-647.04
21	-2721.47912	2.008	-2721.48251	0.924	-2.1272571	-686.54

Table S10. The H-migration potential barriers (kcal·mol^{-1}) for the NVH-0 and NVH-1 along the IRC path, calculated at the B3LYP/6-311G(d,p) Level.

	IRC	NVH-0		NVH-1	
	TS, BS	-1334.80379		-2721.48776	
		Energy	Barrier	Energy	Barrier
BS	1	-1334.79422	-6.01	-2721.48251	-3.29
	2	-1334.79298	-6.78	-2721.48149	-3.93
	3	-1334.79151	-7.71	-2721.48017	-4.76
	4	-1334.78970	-8.84	-2721.47848	-5.82
	5	-1334.78743	-10.27	-2721.47634	-7.17
	6	-1334.78443	-12.15	-2721.47357	-8.90
	7	-1334.78064	-14.53	-2721.47000	-11.14
T	8	-1334.77672	-16.99	-2721.46638	-13.42
	9	-1334.77341	-19.06	-2721.46327	-15.37
	10	-1334.77112	-20.50	-2721.46107	-16.75
	11	-1334.77029	-21.02	-2721.46027	-17.25
	12	-1334.77112	-20.50	-2721.46106	-16.75
	13	-1334.77343	-19.05	-2721.46325	-15.38
	14	-1334.77675	-16.97	-2721.46636	-13.43
BS	15	-1334.78068	-14.50	-2721.47002	-11.13
	16	-1334.78447	-12.12	-2721.47361	-8.88
	17	-1334.78747	-10.24	-2721.47637	-7.15
	18	-1334.78973	-8.82	-2721.47849	-5.82
	19	-1334.79153	-7.69	-2721.48018	-4.76
	20	-1334.79300	-6.77	-2721.48149	-3.93
	21	-1334.79423	-6.00	-2721.48251	-3.29

Table S11. The spin populations of N, C_1, C_2, C_3, and H of the NVH-1 when the H migrates from the C_1-atom to C_2-radical in the minima energy path along the IRC path.

	IRC	N	C_1	C_2	C_3	H
	1	0.002	0.027	0.896	-0.919	0.008
	2	0.002	0.036	0.889	-0.919	0.010
	3	-0.002	0.047	0.880	-0.920	-0.013
BS	4	-0.003	0.063	0.869	-0.922	-0.016
	5	-0.003	0.084	0.853	-0.924	-0.020
	6	-0.004	0.116	0.829	-0.927	-0.025
	7	-0.005	0.163	0.793	-0.932	-0.032
	8	0.008	0.254	0.739	0.938	-0.047
	9	0.004	0.331	0.673	0.937	-0.055
	10	0.002	0.417	0.595	0.936	-0.060
T	11	0.001	0.508	0.508	0.936	-0.062
	12	0.002	0.595	0.418	0.595	-0.060
	13	0.004	0.673	0.331	0.937	-0.055
	14	0.008	0.739	0.254	0.938	-0.047
	15	-0.005	0.793	0.163	-0.932	-0.032
	16	-0.004	0.829	0.117	-0.927	-0.025
	17	-0.003	0.853	0.084	-0.924	-0.020
BS	18	-0.003	0.868	0.063	-0.922	0.016
	19	-0.002	0.880	0.048	-0.920	-0.013
	20	-0.002	0.889	0.036	-0.919	-0.010
	21	-0.002	0.896	0.027	-0.918	-0.008

Table S12(A). The energy levels (eV) of MO(1)α, MO(2)β, MO(3)α, MO(4)β, MO(5)α, and MO(6)β along the BS-IRC path of NVH-0, calculated at the B3LYP/6-311G(d,p) level.

IRC	MO(1)α	MO(2)β	MO(3)α	MO(4)β	MO(5)α	MO(6)β
1	-4.295	-4.302	-8.607	-8.516	-5.365	-5.364
2	-4.292	-4.311	-8.614	-8.511	-5.361	-5.359
3	-4.287	-4.320	-8.614	-8.499	-5.355	-5.352
4	-4.281	-4.324	-8.608	-8.476	-5.344	-5.339
5	-4.271	-4.314	-8.592	-8.437	-5.323	-5.318
6	-4.259	-4.279	-8.574	-8.389	-5.289	-5.288
7	-4.245	-4.223	-8.561	-8.376	-5.250	-5.258
8	-4.229	-4.157	-8.555	-8.376	-5.212	-5.234
9	-4.214	-4.095	-8.556	-8.376	-5.181	-5.218
10	-4.203	-4.051	-8.558	-8.376	-5.161	-5.208
11	-4.199	-4.035	-8.559	-8.377	-5.153	-5.205
12	-4.203	-4.051	-8.558	-8.376	-5.208	-5.161
13	-4.214	-4.095	-8.556	-8.376	-5.218	-5.181
14	-4.229	-4.156	-8.556	-8.376	-5.234	-5.212
15	-4.245	-4.222	-8.562	-8.376	-5.258	-5.250
16	-4.259	-4.279	-8.574	-8.389	-5.288	-5.289
17	-4.272	-4.314	-8.592	-8.438	-5.318	-5.323
18	-4.281	-4.324	-8.608	-8.477	-5.340	-5.344
19	-4.287	-4.319	-8.615	-8.500	-5.352	-5.355
20	-4.292	-4.311	-8.614	-8.512	-5.359	-5.361
21	-4.295	-4.302	-8.608	-8.517	-5.364	-5.366

Table S12(B). The energy levels (eV) of MO(1)α, MO(2)α, MO(3)α, MO(4)β, MO(5)α, and MO(6)β along the T-IRC path of NVH-0, calculated at the B3LYP/6-311G(d,p) level.

IRC	MO(1)α	MO(2)α	MO(3)α	MO(4)β	MO(5)α	MO(6)β
1	-4.106	-4.457	-8.688	-8.469	-5.449	-5.307
2	-4.114	-4.457	-8.690	-8.464	-5.444	-5.302
3	-4.123	-4.455	-8.686	-8.454	-5.437	-5.295
4	-4.132	-4.449	-8.676	-8.433	-5.423	-5.284
5	-4.140	-4.430	-8.658	-8.395	-5.398	-5.264
6	-4.145	-4.390	-8.640	-8.349	-5.361	-5.235
7	-4.143	-4.335	-8.626	-8.345	-5.321	-5.199
8	-4.131	-4.283	-8.619	-8.345	-5.288	-5.165
9	-4.106	-4.248	-8.616	-8.345	-5.263	-5.136
10	-4.080	-4.232	-8.616	-8.345	-5.247	-5.117
11	-4.069	-4.228	-8.617	-8.346	-5.242	-5.110
12	-4.080	-4.232	-8.617	-8.346	-5.247	-5.117
13	-4.106	-4.248	-8.617	-8.345	-5.263	-5.136
14	-4.131	-4.283	-8.620	-8.345	-5.288	-5.165
15	-4.143	-4.335	-8.627	-8.345	-5.321	-5.199
16	-4.145	-4.389	-8.640	-8.349	-5.361	-5.235
17	-4.140	-4.430	-8.659	-8.396	-5.398	-5.264
18	-4.132	-4.449	-8.676	-8.434	-5.423	-5.284
19	-4.123	-4.455	-8.686	-8.455	-5.437	-5.295
20	-4.114	-4.457	-8.690	-8.465	-5.444	-5.302
21	-4.106	-4.457	-8.689	-8.469	-5.450	-5.307

Table S12(C). The energy levels (eV) of MO(1)α, MO(2)β, MO(3)α, MO(4)β, MO(5)α, and MO(6)β along the BS-IRC path of NVH-1, calculated at the B3LYP/6-311G(d,p) level.

IRC	MO(1)α	MO(2)β	MO(3)α	MO(4)β	MO(5)α	MO(6)β
1	-3.904	-3.911	-7.583	-7.609	-4.947	-4.928
2	-3.921	-3.900	-7.611	-7.580	-4.924	-4.943
3	-3.931	-3.894	-7.609	-7.571	-4.919	-4.939
4	-3.938	-3.885	-7.602	-7.556	-4.909	-4.930
5	-3.934	-3.874	-7.590	-7.532	-4.891	-4.912
6	-3.910	-3.857	-7.577	-7.503	-4.863	-4.879
7	-3.862	-3.836	-7.571	-7.475	-4.833	-4.836
8	-3.802	-3.811	-7.571	-7.453	-4.809	-4.794
9	-3.744	-3.787	-7.576	-7.438	-4.793	-4.759
10	-3.713	-3.773	-7.57	-7.428	-4.725	-4.725
11	-3.695	-3.759	-7.579	-7.426	-4.727	-4.727
12	-3.714	-3.774	-7.577	-7.428	-4.725	-4.725
13	-3.744	-3.787	-7.576	-7.438	-4.793	-4.759
14	-3.802	-3.812	-7.571	-7.453	-4.809	-4.794
15	-3.862	-3.836	-7.571	-7.475	-4.833	-4.836
16	-3.909	-3.858	-7.578	-7.503	-4.864	-4.879
17	-3.934	-3.874	-7.590	-7.533	-4.892	-4.912
18	-3.937	-3.886	-7.602	-7.556	-4.909	-4.930
19	-3.931	-3.894	-7.610	-7.572	-4.919	-4.939
20	-3.921	-3.900	-7.611	-7.580	-4.925	-4.944
21	-3.910	-3.905	-7.609	-7.583	-4.928	-4.946

Table S12(D). The energy levels (eV) of MO(1)α, MO(2)α, MO(3)α, MO(4)β, MO(5)α, and MO(6)β along the T-IRC path of NVH-1, calculated at the B3LYP/6-311G(d,p) level.

IRC	MO(1)α	MO(2)α	MO(3)α	MO(4)β	MO(5)α	MO(6)β
1	-3.667	-4.081	-7.678	-7.545	-5.035	-4.879
2	-3.680	-4.082	-7.679	-7.542	-5.029	-4.874
3	-3.692	-4.083	-7.677	-7.536	-5.023	-4.868
4	-3.705	-4.079	-7.669	-7.523	-5.012	-4.858
5	-3.718	-4.065	-7.658	-7.501	-4.992	-4.841
6	-3.730	-4.031	-7.646	-7.471	-4.958	-4.812
7	-3.740	-3.977	-7.640	-7.439	-4.915	-4.773
8	-3.746	-3.915	-7.639	-7.411	-4.877	-4.734
9	-3.747	-3.859	-7.640	-7.390	-4.848	-4.700
10	-3.742	-3.824	-7.643	-7.377	-4.830	-4.678
11	-3.738	-3.813	-7.644	-7.372	-4.823	-4.670
12	-3.741	-3.824	-7.643	-7.377	-4.830	-4.678
13	-3.746	-3.860	-7.641	-7.390	-4.848	-4.700
14	-3.745	-3.915	-7.639	-7.412	-4.877	-4.734
15	-3.739	-3.977	-7.640	-7.439	-4.915	-4.773
16	-3.729	-4.032	-7.647	-7.471	-4.958	-4.812
17	-3.717	-4.065	-7.658	-7.501	-4.993	-4.841
18	-3.704	-4.079	-7.670	-7.523	-5.013	-4.858
19	-3.692	-4.083	-7.677	-7.536	-5.023	-4.868
20	-3.679	-4.083	-7.680	-7.543	-5.030	-4.875
21	-3.667	-4.080	-7.679	-7.544	-5.033	-4.878

Table S12(E). The energy gaps of two SOMOs (MO(1)α, MO(2)α) in the T state changing along the T-IRC path of NVH-0 and NVH-1, calculated at the B3LYP/6-311G(d,p) level.

	NVH-0			NVH-1		
IRC	**MO(1)α**	**MO(2)α**	**Gap**	**MO(1)α**	**MO(2)α**	**Gap**
1	-4.106	-4.457	0.351	-3.667	-4.081	0.414
2	-4.114	-4.457	0.343	-3.680	-4.082	0.402
3	-4.123	-4.455	0.332	-3.692	-4.083	0.391
4	-4.132	-4.449	0.317	-3.705	-4.079	0.374
5	-4.140	-4.430	0.290	-3.718	-4.065	0.347
6	-4.145	-4.390	0.245	-3.730	-4.031	0.301
7	-4.143	-4.335	0.192	-3.740	-3.977	0.237
8	-4.131	-4.283	0.152	-3.746	-3.915	0.169
9	-4.106	-4.248	0.142	-3.747	-3.859	0.112
10	-4.080	-4.232	0.152	-3.742	-3.824	0.082
11	-4.069	-4.228	0.159	-3.738	-3.813	0.075
12	-4.080	-4.232	0.152	-3.741	-3.824	0.083
13	-4.106	-4.248	0.142	-3.746	-3.860	0.114
14	-4.131	-4.283	0.152	-3.745	-3.915	0.170
15	-4.143	-4.335	0.192	-3.739	-3.977	0.238
16	-4.145	-4.389	0.244	-3.729	-4.032	0.303
17	-4.140	-4.430	0.290	-3.717	-4.065	0.348
18	-4.132	-4.449	0.317	-3.704	-4.079	0.375
19	-4.123	-4.455	0.332	-3.692	-4.083	0.391
20	-4.114	-4.457	0.343	-3.679	-4.083	0.404
21	-4.106	-4.457	0.351	-3.667	-4.080	0.413

Table S12(F). The energy gaps of two SOMOs (MO(1)α, MO(2)β) in the BS state changing along the BS-IRC path of NVH-0 and NVH-1, calculated at the B3LYP/6-311G(d,p) level.

	NVH-0			NVH-1		
IRC	**MO(1)α**	**MO(2)β**	**Gap**	**MO(1)α**	**MO(2)β**	**Gap**
1	-4.295	-4.302	-0.007	-3.904	-3.911	-0.007
2	-4.292	-4.311	-0.019	-3.921	-3.900	0.021
3	-4.287	-4.320	-0.033	-3.931	-3.894	0.037
4	-4.281	-4.324	-0.043	-3.938	-3.885	0.053
5	-4.271	-4.314	-0.043	-3.934	-3.874	0.060
6	-4.259	-4.279	-0.020	-3.910	-3.857	0.053
7	-4.245	-4.223	0.022	-3.862	-3.836	0.026
8	-4.229	-4.157	0.072	-3.802	-3.811	-0.009
9	-4.214	-4.095	0.119	-3.744	-3.787	-0.043
10	-4.203	-4.051	0.152	-3.713	-3.773	-0.060
11	-4.199	-4.035	0.164	-3.695	-3.759	-0.064
12	-4.203	-4.051	0.152	-3.714	-3.774	-0.060
13	-4.214	-4.095	0.119	-3.744	-3.787	-0.043
14	-4.229	-4.156	0.073	-3.802	-3.812	-0.010
15	-4.245	-4.222	0.023	-3.862	-3.836	0.026
16	-4.259	-4.279	-0.020	-3.909	-3.858	0.051
17	-4.272	-4.314	-0.042	-3.934	-3.874	0.060
18	-4.281	-4.324	-0.043	-3.937	-3.886	0.051
19	-4.287	-4.319	-0.032	-3.931	-3.894	0.037
20	-4.292	-4.311	-0.019	-3.921	-3.900	0.021
21	-4.295	-4.302	-0.007	-3.910	-3.905	0.005

Table S13(A). The singly occupied molecular orbitals (three C and one H, isovalue = 0.1) and spin density distributions (isovalue = 0.01) of SP1-SP11(TS) on the BS-IRC path of NVH-0, calculated at the B3LYP/6-311G(d,p) level.

	MO(1)α	MO(2)β	MO(3)α	MO(4)β	Spin Density
Initial, BS	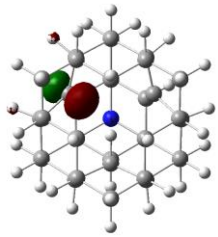	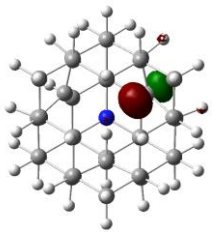	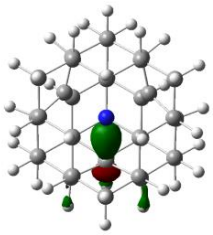	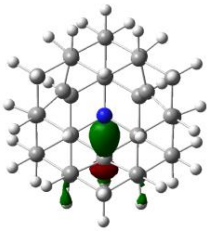	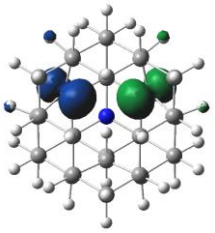
SP1, BS	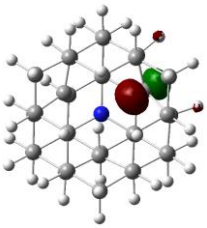	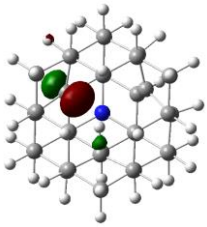	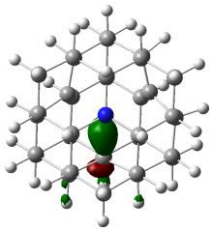	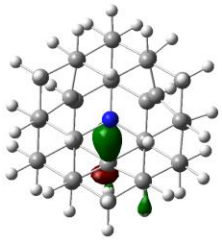	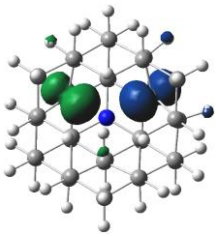
SP2, BS	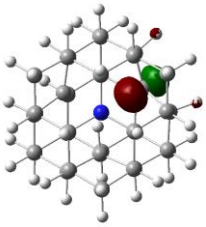	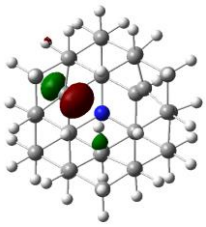	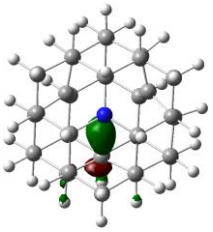	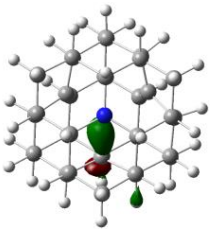	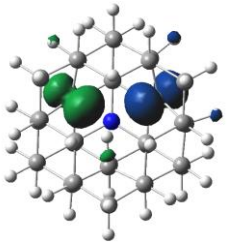
SP3, BS	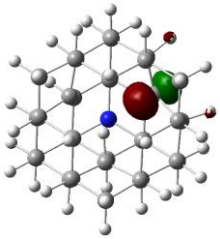	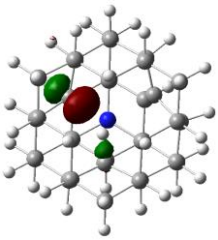	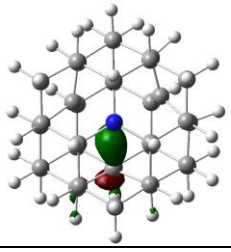	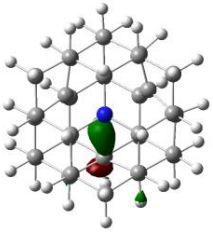	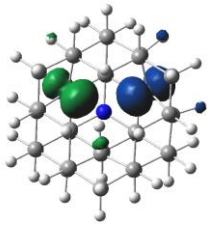
SP4, BS	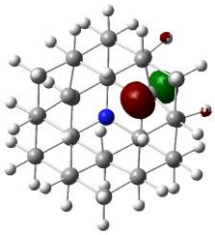	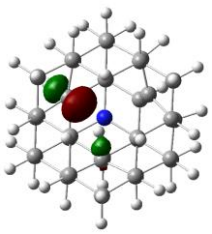	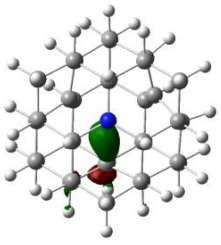	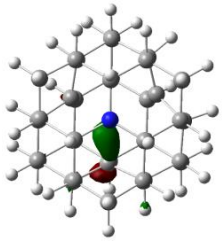	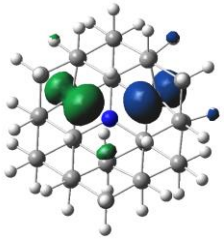
SP5, BS	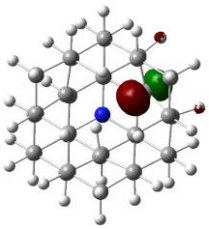	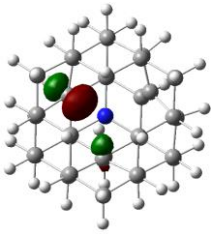	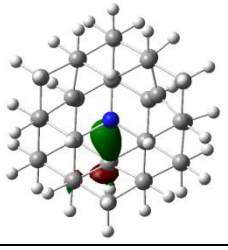	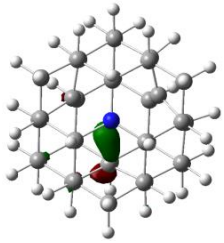	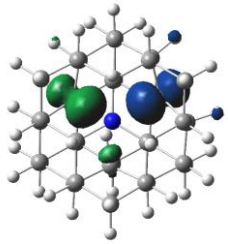

SP6, BS	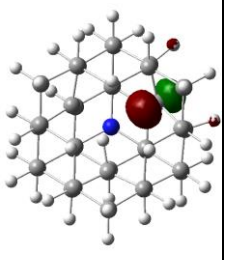	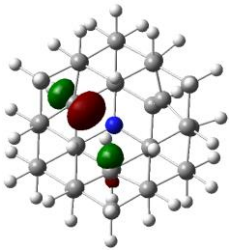	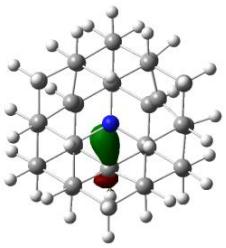	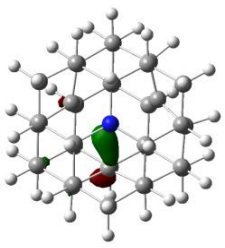	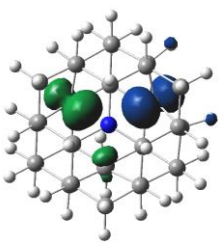
SP7, BS	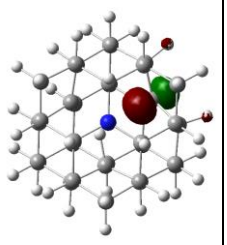	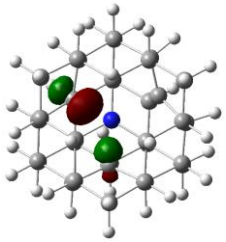	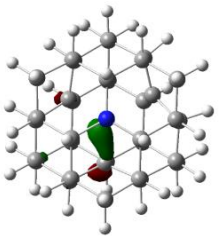	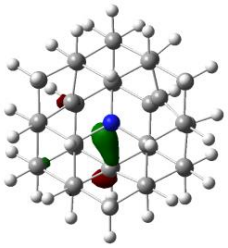	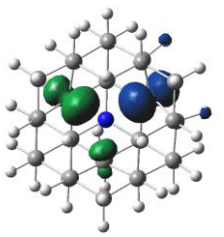
SP8, BS	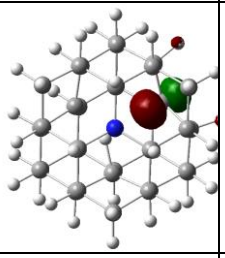	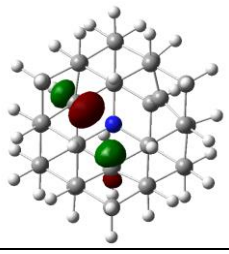	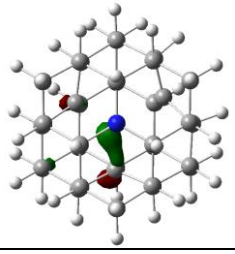	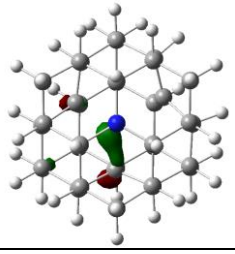	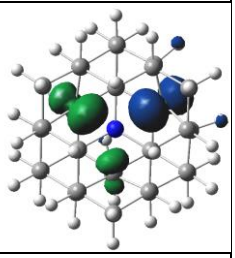
SP9, BS	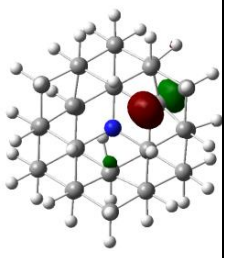	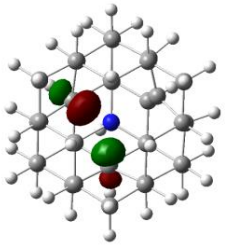	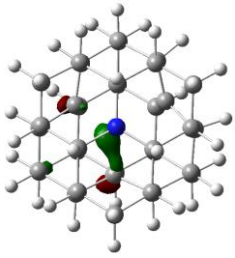	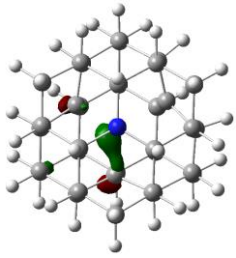	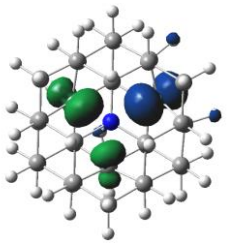
SP10, BS	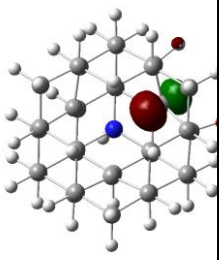	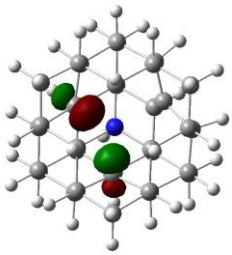	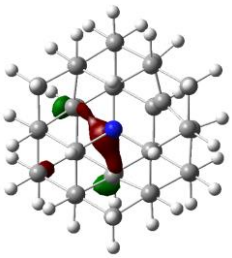	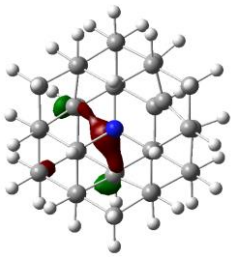	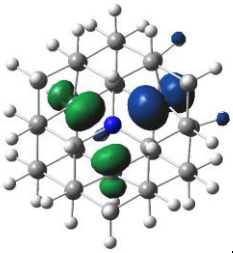
SP11, BS	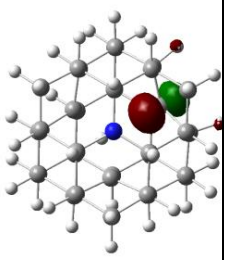	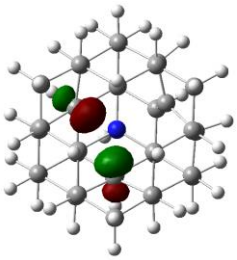	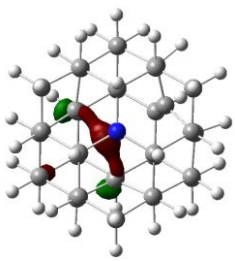	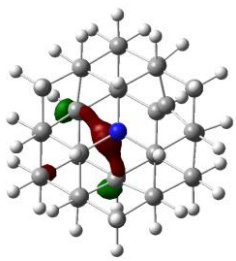	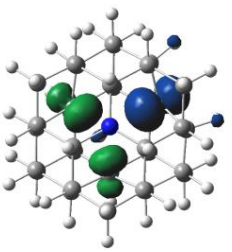

Table S13(B). The singly occupied molecular orbitals (three C and one H, isovalue = 0.1) and spin density distributions (isovalue = 0.01) of SP1-SP11(TS) on the T-IRC path of the NVH-0, calculated at the B3LYP/6-311G(d,p) level.

	MO(1)α	MO(2) α	MO(3)α	MO(4)β	Spin Density
Initial, T	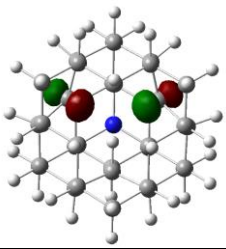	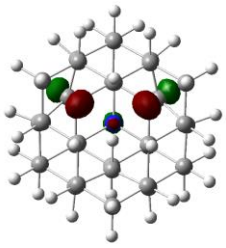	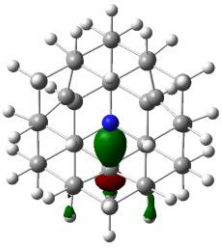	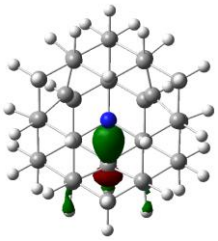	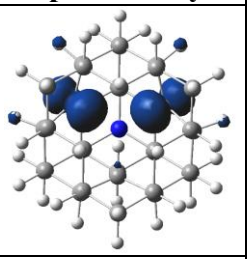
SP1, T	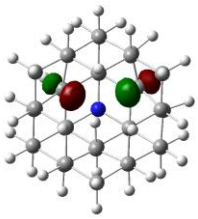	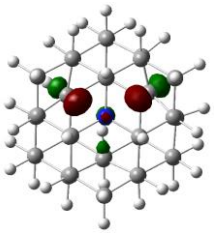	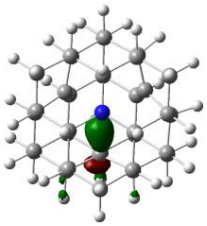	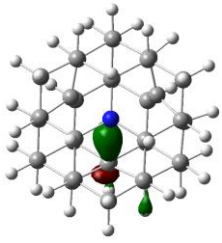	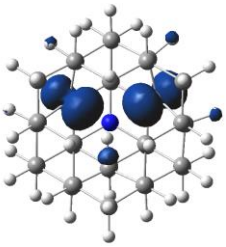
SP2, T	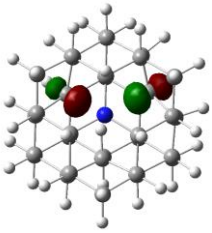	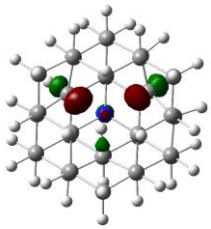	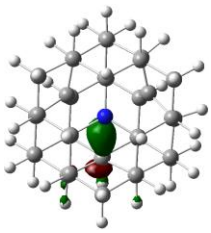	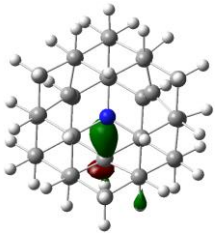	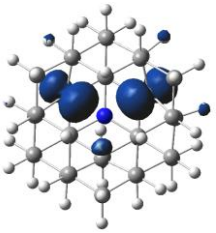
SP3, T	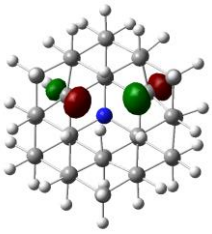	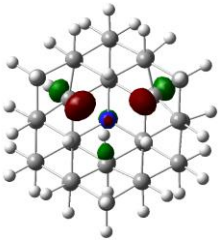	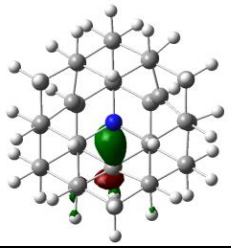	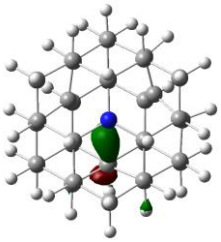	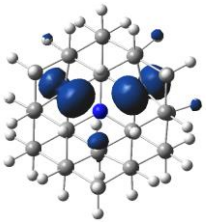
SP4, T	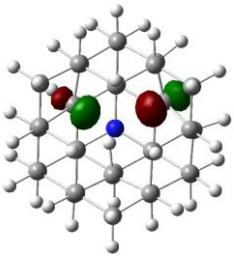	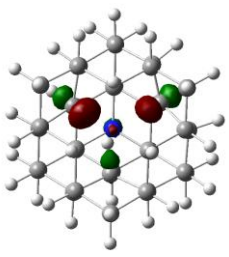	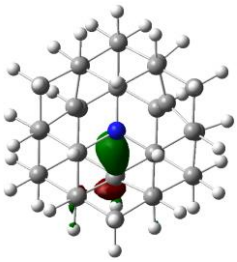	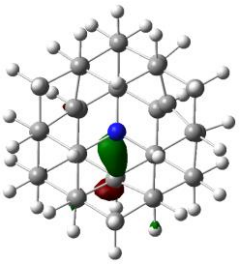	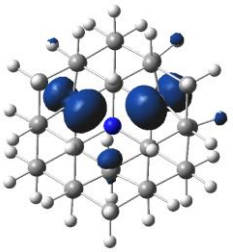
SP5, T	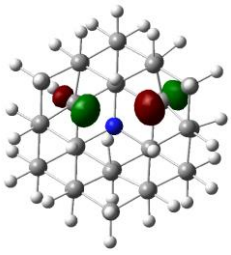	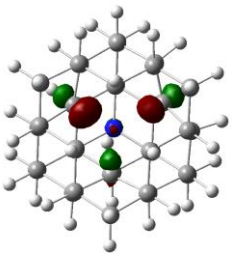	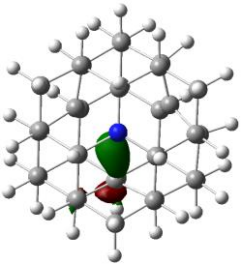	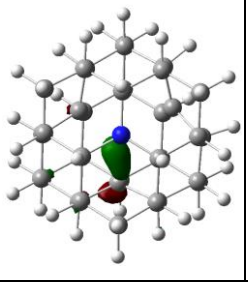	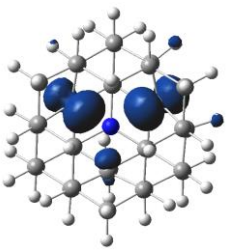

SP6, T	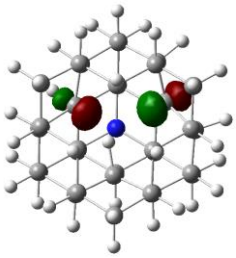	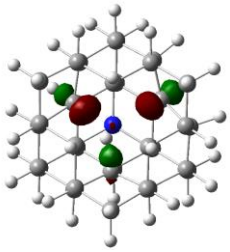	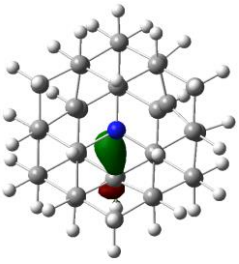	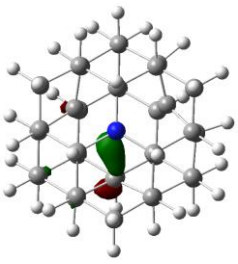	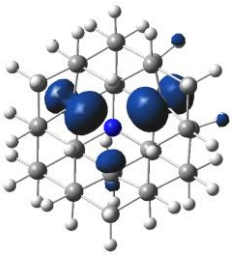
SP7, T	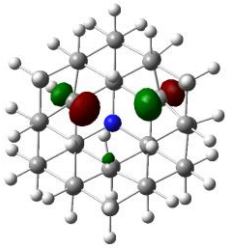	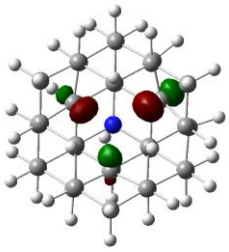	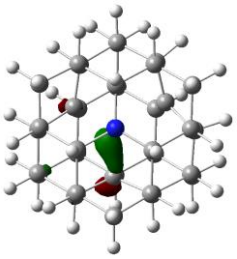	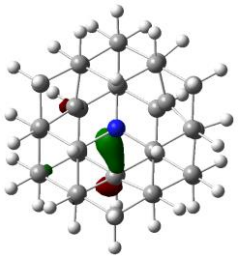	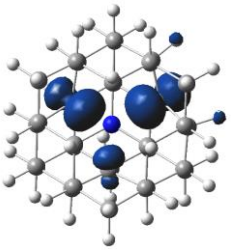
SP8, T	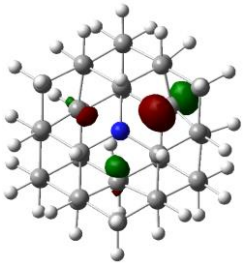	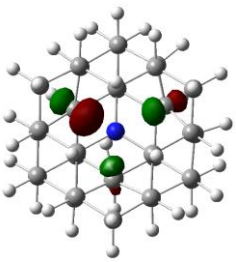	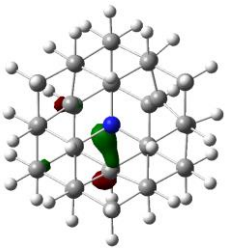	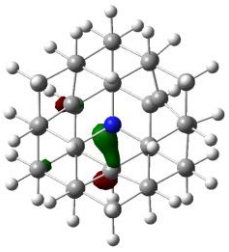	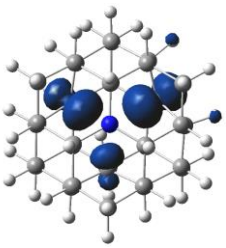
SP9, T	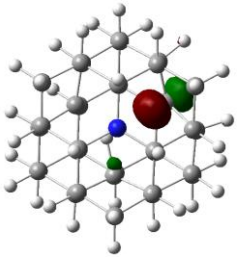	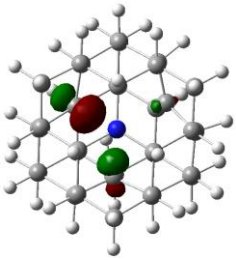	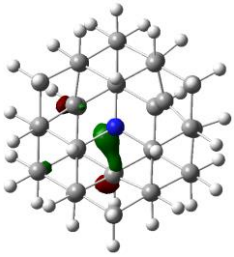	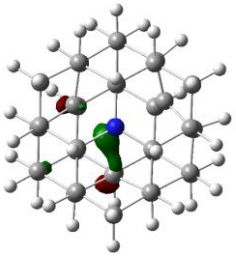	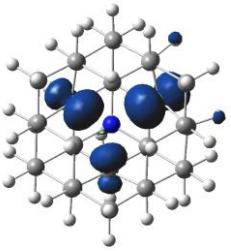
SP10, T	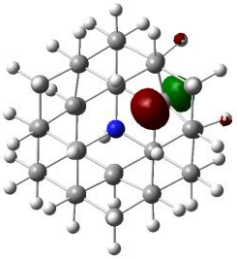	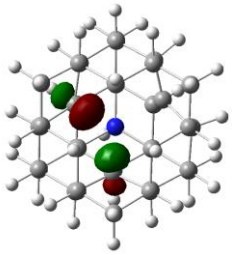	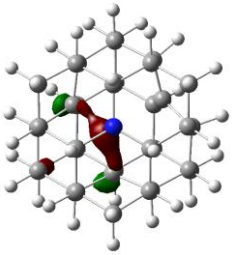	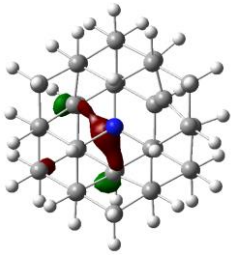	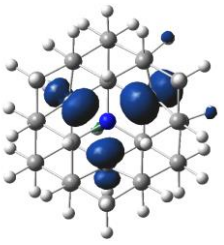
SP11, T	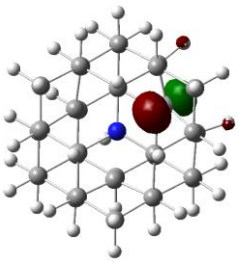	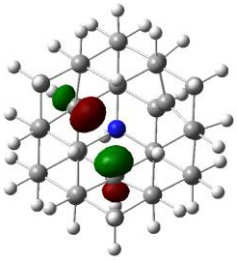	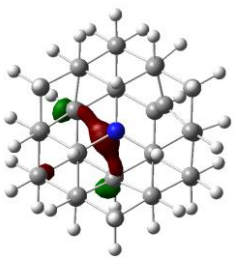	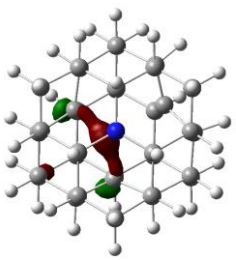	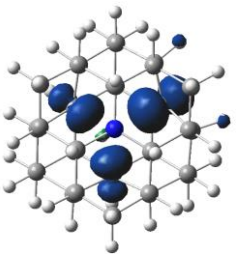

Table S13(C). The singly occupied molecular orbitals (three C and one H, isovalue = 0.1) and spin density distributions (isovalue = 0.01) of SP1-SP11(TS) on the BS-IRC path of the NVH-1, calculated at the B3LYP/6-311G(d,p) level.

	MO(1)α	MO(2)β	MO(3)α	MO(4)β	Spin Density
Initial, BS	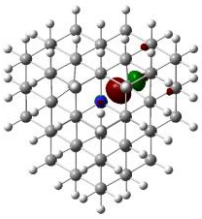	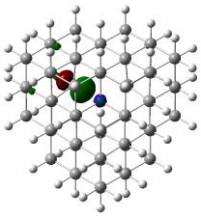	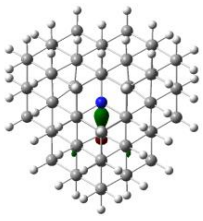	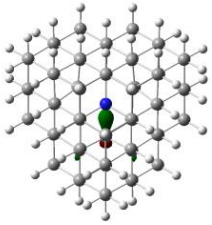	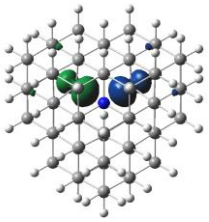
SP1, BS	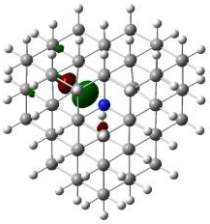	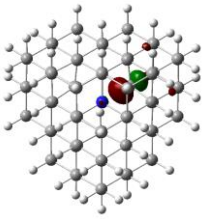	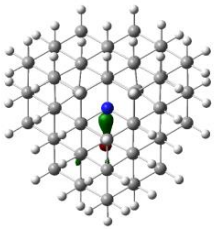	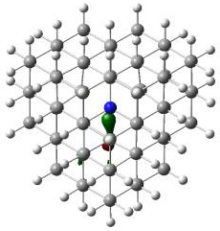	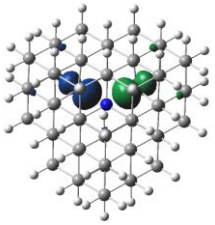
SP2, BS	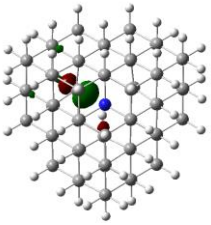	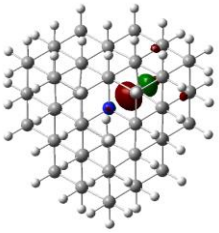	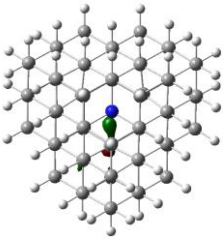	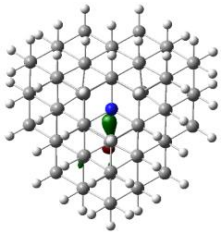	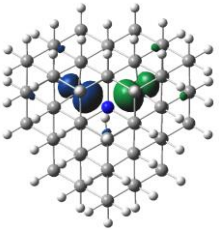
SP3, BS	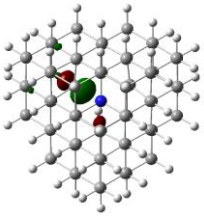	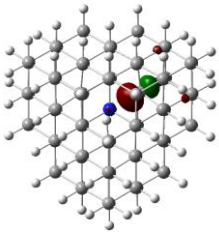	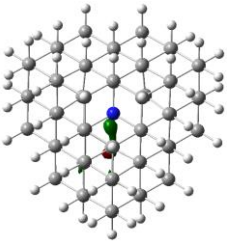	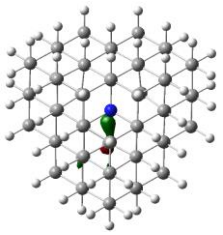	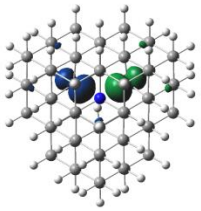
SP4, BS	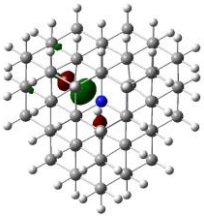	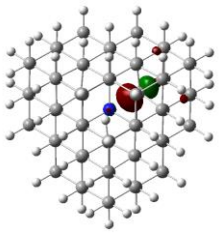	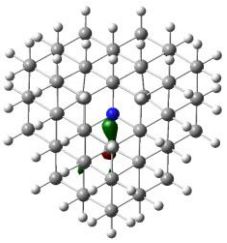	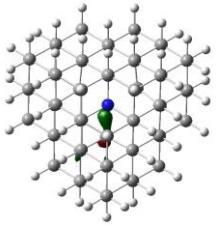	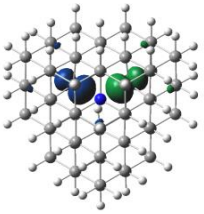
SP5, BS	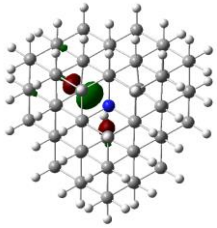	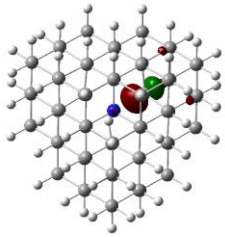	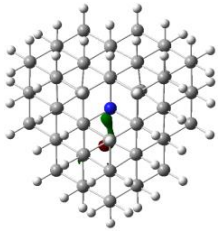	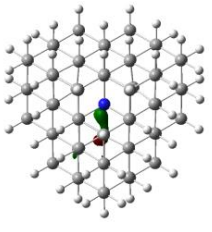	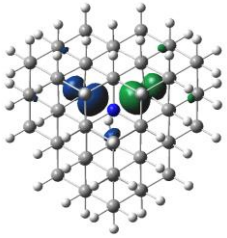

SP6, BS	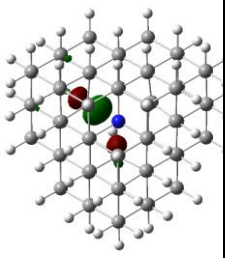	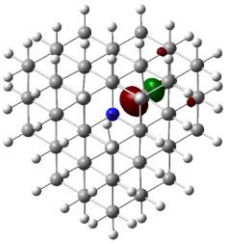	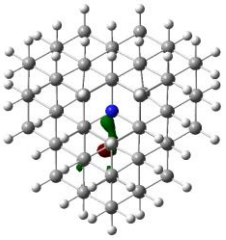	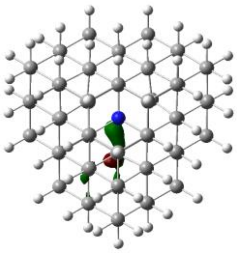	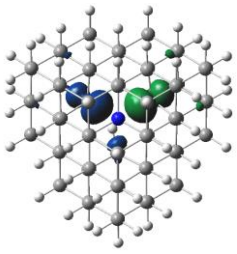
SP7, BS	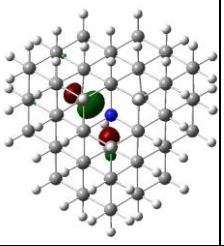	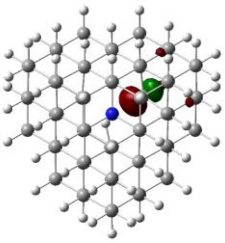	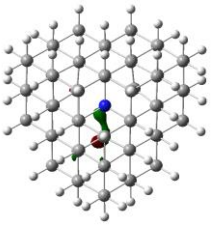	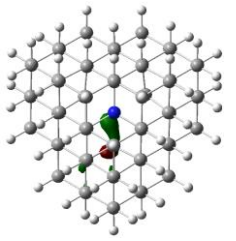	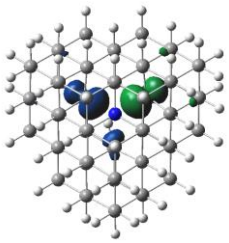
SP8, BS	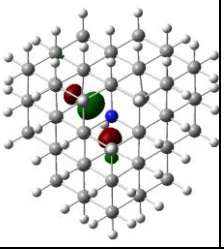	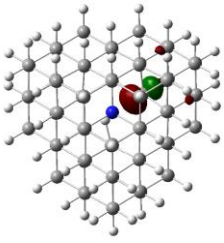	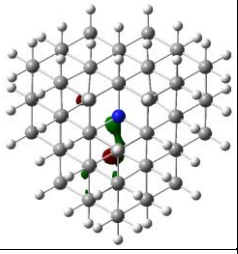	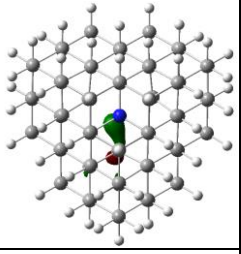	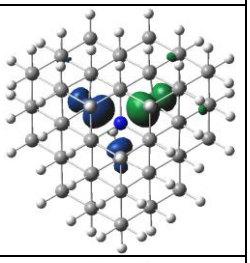
SP9, BS	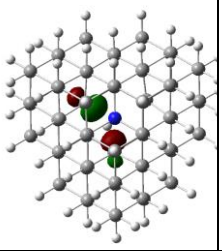	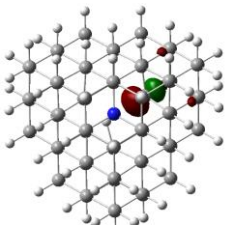	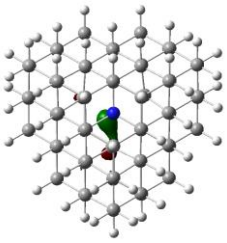	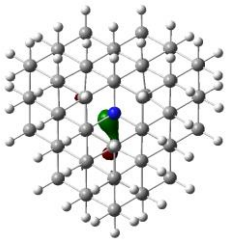	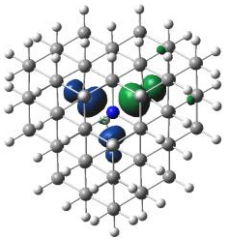
SP10, BS	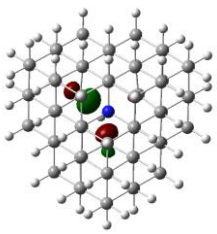	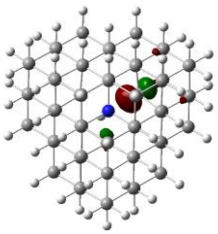	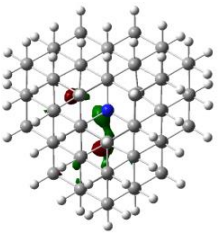	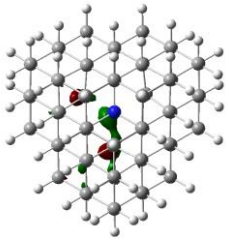	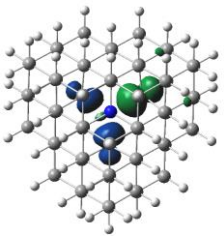
SP11, BS	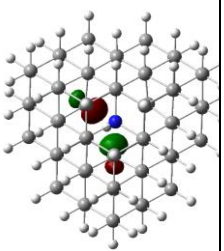	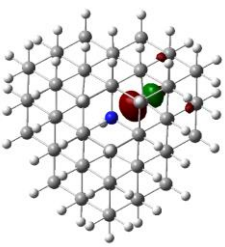	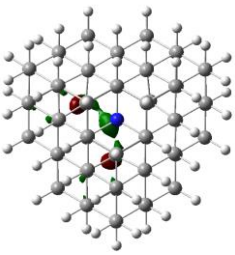	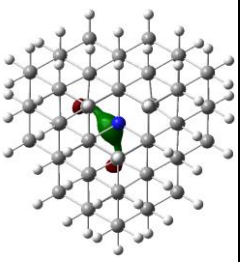	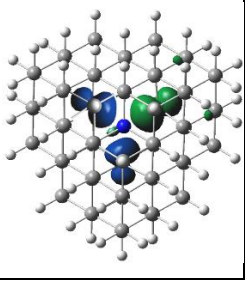

Table S13(D). The singly occupied molecular orbitals (three C and one H, isovalue = 0.1) and spin density distributions (isovalue = 0.01) of SP1-SP11(TS) on the T-IRC path of the NVH-1, calculated at the B3LYP/6-311G(d,p) level.

	MO(1)α	MO(2) α	MO(3)α	MO(4)β	Spin Density
Initial, T	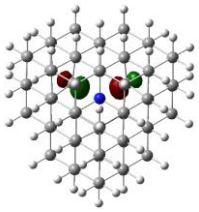	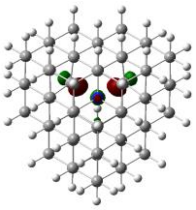	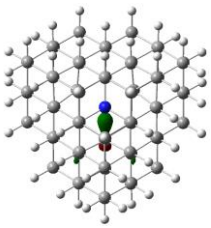	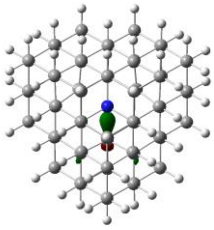	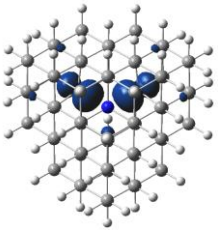
SP1, T	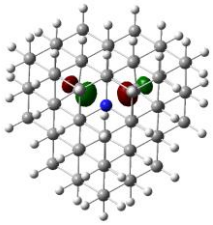	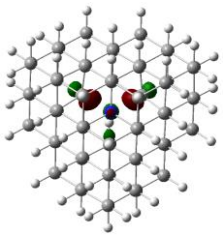	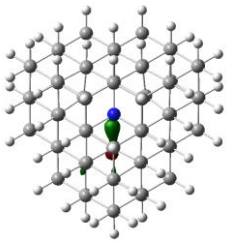	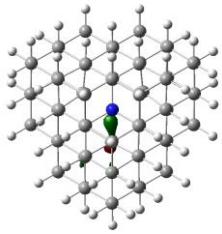	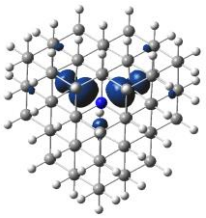
SP2, T	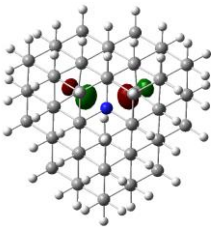	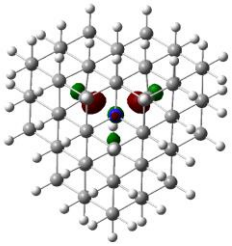	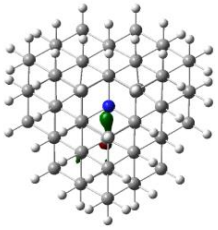	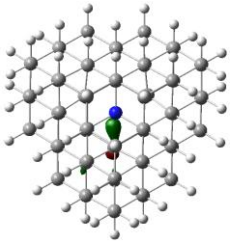	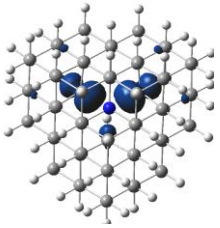
SP3, T	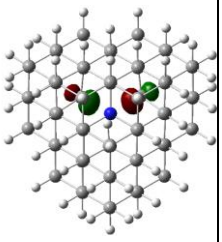	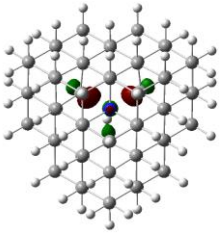	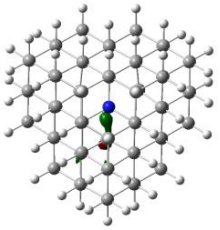	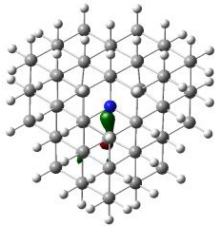	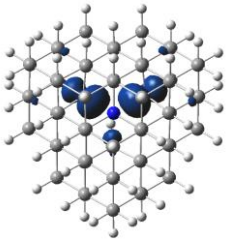
SP4, T	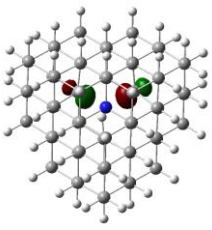	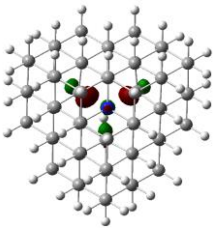	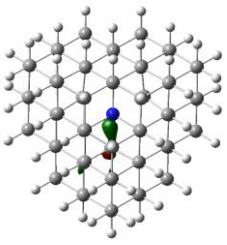	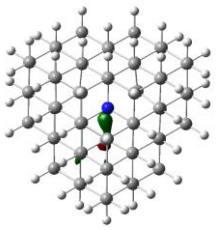	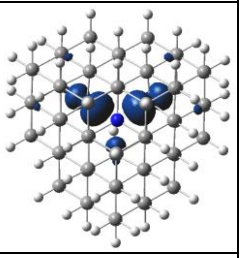
SP5, T	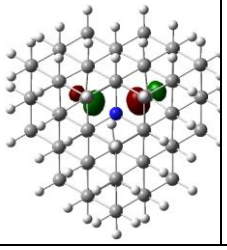	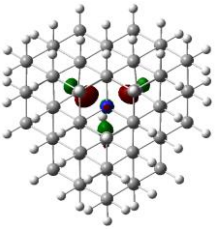	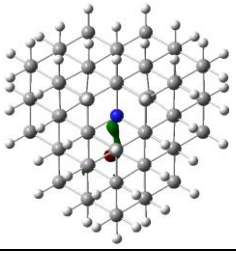	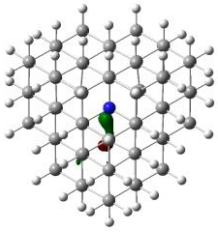	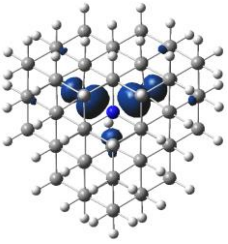

SP6, T	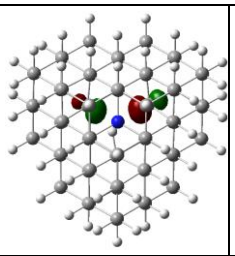	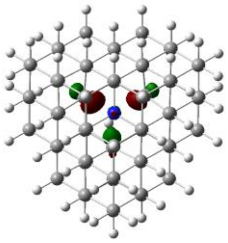	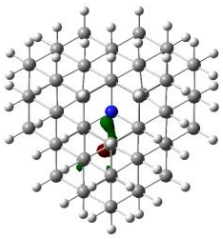	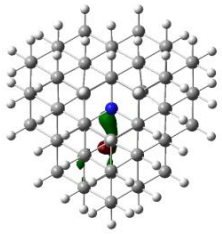	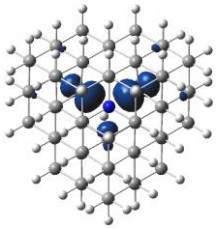
SP7, T	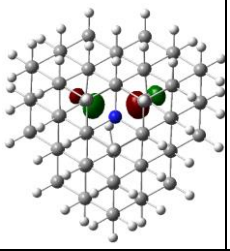	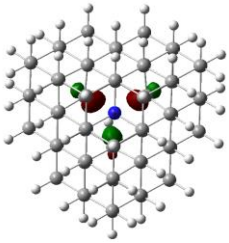	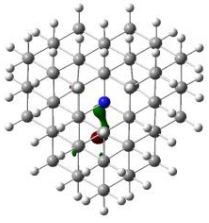	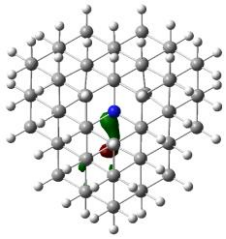	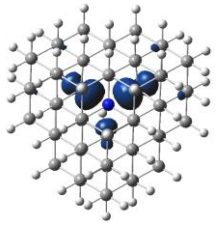
SP8, T	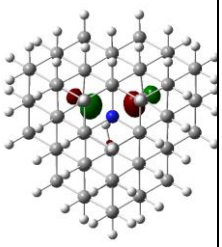	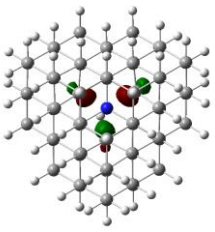	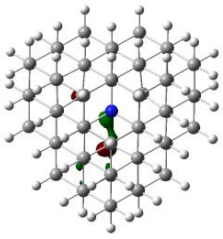	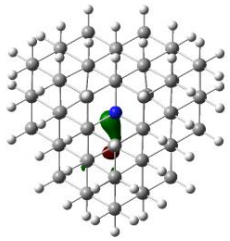	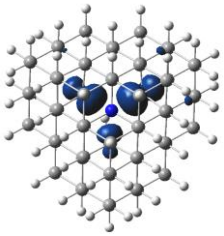
SP9, T	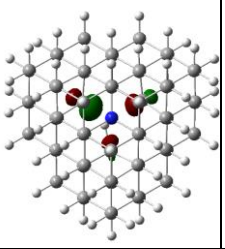	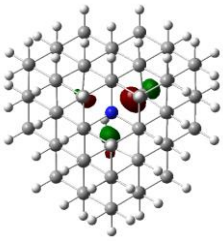	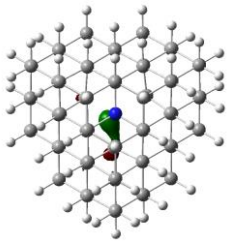	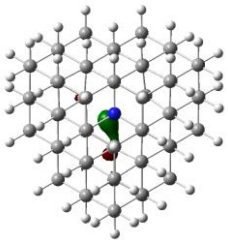	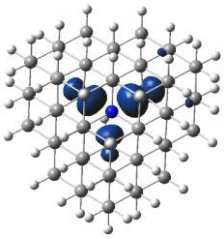
SP10, T	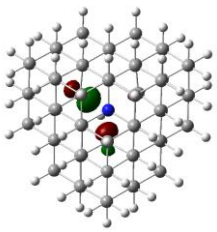	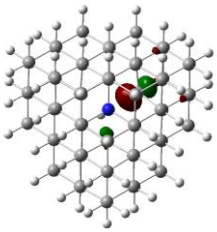	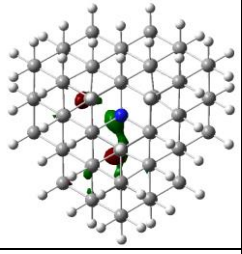	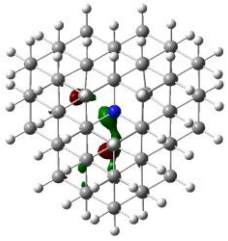	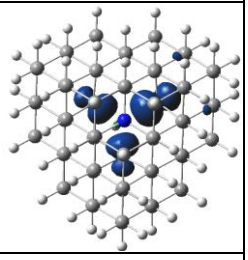
SP11, T	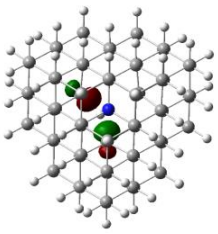	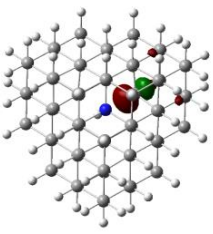	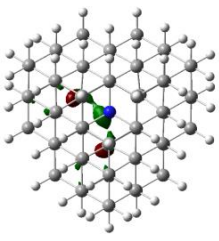	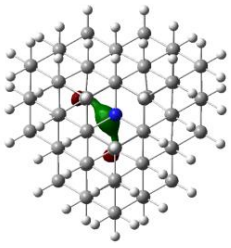	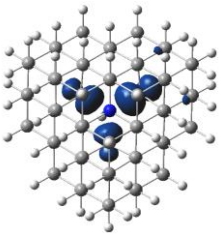

Table S13(E). The singly occupied molecular orbitals of two lone pair electron on N (isovalue = 0.1) of the NVH-0 and NVH-1 of SP1-SP11(TS) in minima energy path along the IRC path, calculated at the B3LYP/6-311G(d,p) level.

	NVH-0		**NVH-1**	
	MO(5)α	**MO(6)β**	**MO(5)α**	**MO(6)β**
Initial, BS	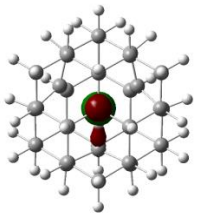	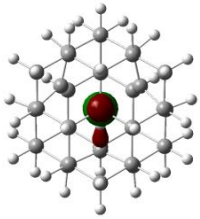	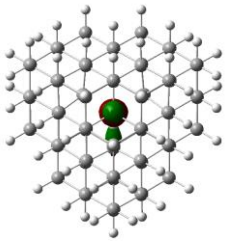	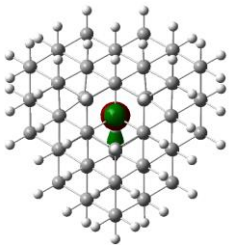
SP1, BS	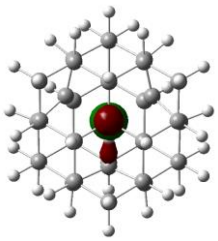	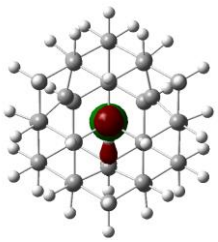	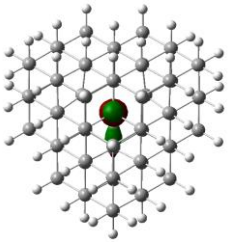	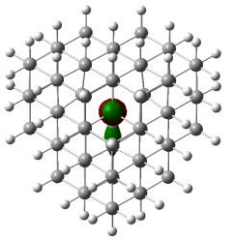
SP2, BS	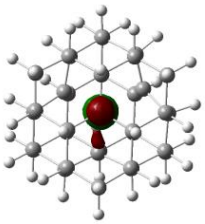	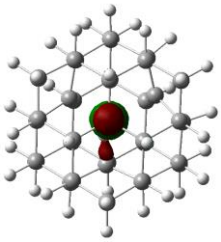	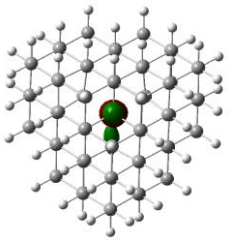	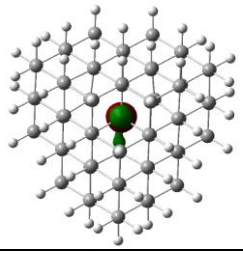
SP3, BS	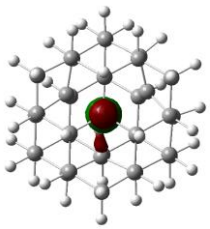	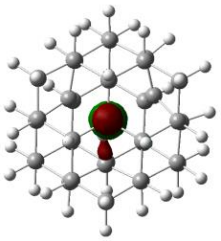	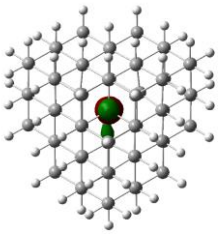	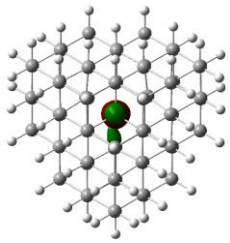
SP4, BS	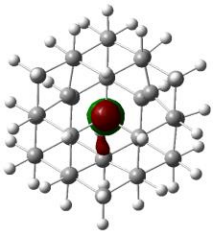	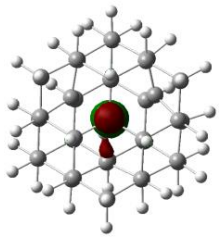	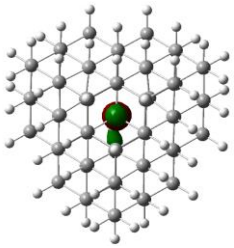	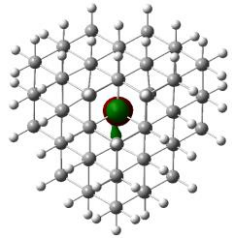
SP5, BS	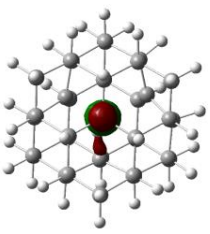	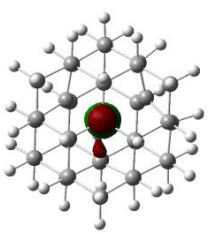	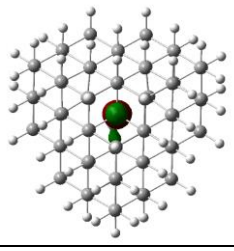	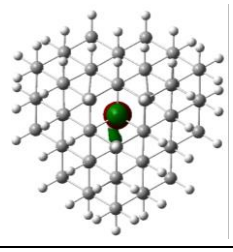

SP6, BS	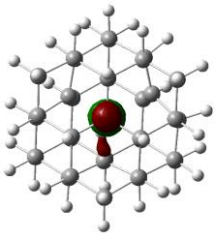	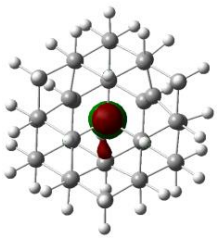	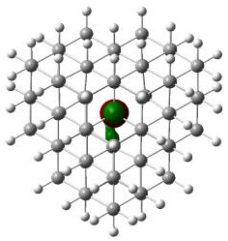	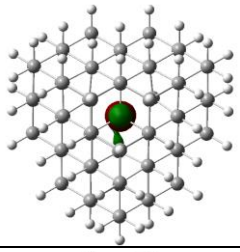
SP7, BS	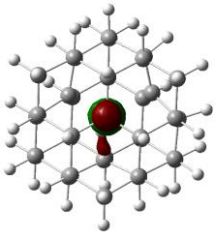	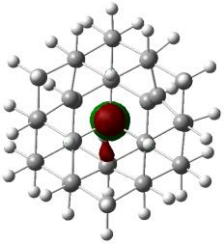	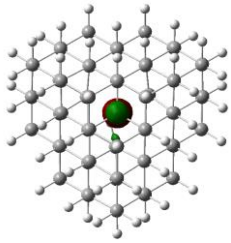	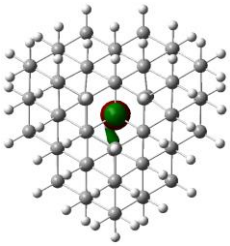
SP8, T	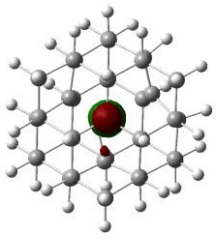	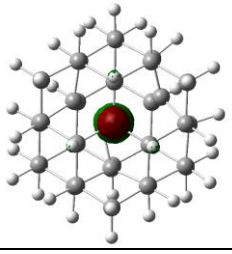	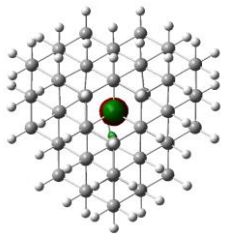	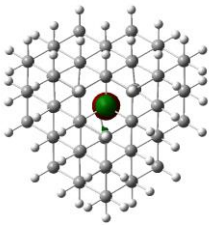
SP9, T	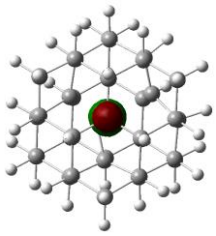	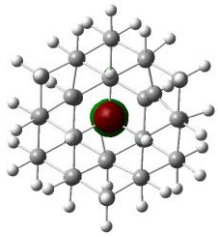	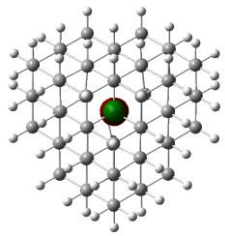	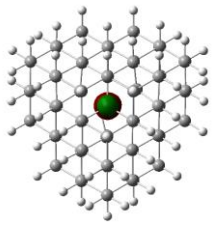
SP10, T	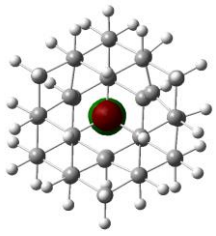	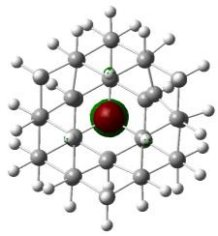	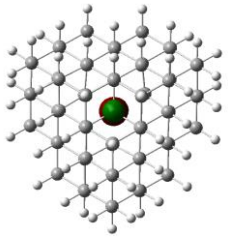	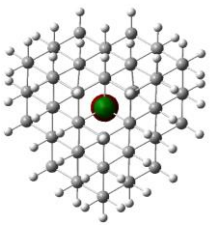
SP11, T	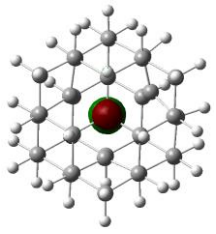	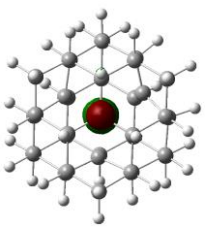	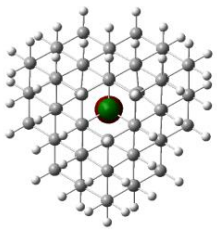	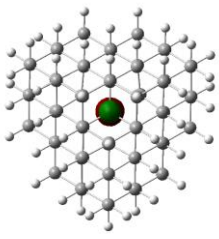

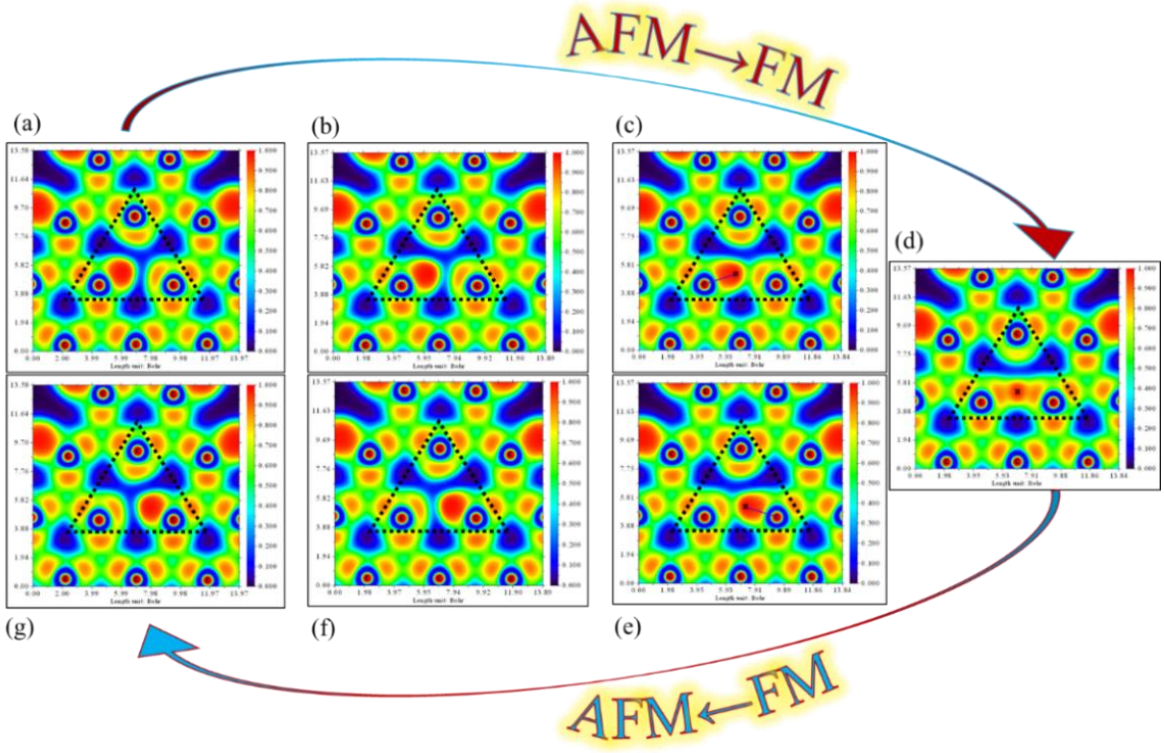

Figure S13. Electron localization function (ELF), calculated with three suspended C-radicals as cross section along the IRC path.

7. Metadynamics Simulation for the NVH Center

Actually, H-transfer dynamics doesn't completely follow the IRC minimum energy pathway, and possible position fluctuation dynamics deviating from minimum energy pathway could lead to an expanded distribution of magnetic coupling strength. To deeply understand how the H-transfer dynamics affects the magnetic coupling inside the tetrahedral space, we explore the H-reachable region through enhanced sampling dynamics simulation and obtain the H-transfer free energy surface. As known, metadynamics is a powerful technique through enhancing sampling in molecular dynamics simulations to reveal how a reaction takes place at the atomic level by taking different sets of collective variables (CV).[1-6] Here, we sample the $C_1\cdots H$ distance as CV1 and the $C_2\cdots H$ distance as CV2. The obtained free energy surface reveals two equivalent minima (Int-1 and Int-2) and their connected one TS on the minimum energy pathway (Figure 5(a)). Calculations confirm that the $E_{BS}<E_T<E_{CS}$ order for both Int-1 and Int-2 and the $E_T<E_{BS}<E_{CS}<E_Q$ order for TS agree well with the optimized results (Table S14). The extracted

activation barrier (ca. 15.14 kcal·mol^{-1}) and calculated J (-883.00/-909.29 cm^{-1} for Int-1/Int-2 and 430.59 cm^{-1} for TS), also nicely agree with the optimized results (17.25 kcal·mol^{-1}, -887.61 cm^{-1}/NVH-1 and 401.03 cm^{-1}/NVH-1(TS), Table S15).

Figure 5(b) shows time evolution of the $C_1\cdots H/C_2\cdots H/C_3\cdots H$ distances (Å) from the metadynamics in a 50 ps dynamics trajectory which clearly reflects the H-transfer dynamics behavior in early three representative time periods (I, II, and III). In Period I (i.e. the initial 15 ps), the C_1-H distance basically keeps around its equilibrium value (1.1 Å), while the $C_2\cdots H$ distance varies around 1.5-3.5 Å with a relatively large amplitude, revealing the H swing dynamics in the Int-1 region. Interestingly, the enhanced sampling reveals a H-transfer tendency towards C_2, as evidenced by frequently observed reduced $C_2\cdots H$ distance (ca. 1.5 Å). At ca. 15 ps, the H enters the Int-2 region and swings around C_2 in a subsequent time period (i.e. Period II, ca. 15-32 ps), as evidenced by the C_2-H (ca. 1.1 Å) and $C_1\cdots H$ distances (ca. 1.5-3.5 Å). This observation clearly indicates a successful H-transfer from the C_1 to C_2 region at ca. 15 ps, as confirmed by the evolution detail in Figure S16(b) (the 14.9-15.1 ps period). The extracted $C_1\cdots H$ distance from free energy surface for the intersection point is 1.372 Å which is highly consistent with that (1.372 Å) from IRC minimum energy pathway. At ca. 32 ps, the proton transfers back the Int-1 region and continues to swing around C_1 with the $C_1\cdots H$ distance of ca. 1.1 Å in the next time period (Period III, ca. 32-39 ps).

We statistically check the $C_1\cdots H$ distances of all transient configurations in metadynamics and observe a bimodal distribution with two peaks at 1.0-1.2 Å and 1.9-2.1 Å which reflect the proton dynamics around C_1 and C_2 on free energy surface, respectively (Figure 5(c)). The valley corresponds to the TS region. The J values of all transient configurations present a high quasi-linear correlation with the $C_1\cdots H$ distance (Figure 5(d)). Interestingly, this correlation line can be divided into two regions where $J < 0$ (the AFM coupling) for the $C_1\cdots H$ distance in 1.0-1.2 Å and $J > 0$ (the FM coupling) in 1.2-1.4 Å (the region close to TS), and the $C_1\cdots H$ distance of ca. 1.2 Å is a magnetic switching boundary between AFM and FM. Clearly, Figure 5(c,d) and Table S8 indicate that H-transfer dynamics exhibits large probabilities in two traps around C_1 and C_2, respectively, and thus large probability of the AFM coupling, while it has small probability at the middle region (the TS one) and the FM coupling. Intriguingly, the magnetic couplings

from the metadynamics exhibits a larger value distribution from -1281.89 cm^{-1} (AFM) to 597.93 cm^{-1} (FM) than those (-887.61 cm^{-1} to 401.03 cm^{-1}) from the IRC minimum energy pathway calculations (Table S17). This observation confirms that H-transfer dynamics can govern the magnetic coupling with a large fluctuation and frequent switching.

References

1. Laio, A.; Parrinello, M. Escaping Free Energy Minima. *Proc. Natl. Acad. Sci. USA* **2002**, *99*, 12562–12566.
2. Barducci, A.; Bonomi, M.; Parrinello, M. Metadynamics. *WIREs. Comput. Mol. Sci.* **2011**, *1(5)*, 826-843.
3. Tiwary, P.; Parrinello, M. From Metadynamics to Dynamics. *Phys. Rev. Lett.* **2013**, *111(23)*, 230602.
4. Bussi, G.; Laio, A. Using Metadynamics to Explore Complex Free-Energy Landscapes. *Nat. Rev. Phys.* **2020**, *2(4)*, 200-212.
5. Sutto, L.; Marsili, S.; Gervasio, F. L. New Advances in Metadynamics. *WIREs. Comput. Mol. Sci.* **2012**, *2(5)*, 771-779.
6. Barducci, A.; Bussi, G.; Parrinello, M. Well-tempered Metadynamics: A Smoothly Converging and Tunable Free-Energy Method. *Phys. Rev. Lett.* **2008**, *100(2)*, 020603.

Table S14. Energies in the BS、T、CS, and Q states of the NVH-1 in two minima location (Int1 and Int2) and TS obtained from the free energy surface, calculated at the B3LYP/6-311G(d,p).

Diamond	**E_{BS}/(a.u.)**	**E_T/(a.u.)**	**E_{CS}/(a.u.)**	**E_Q/(a.u.)**
Int1	-2721.25725	-2721.25342	-2721.24833	
Int2	-2721.25517	-2721.25122	-2721.24687	
TS	-2721.23013	-2721.23209	-2721.22770	-2721.22353

Table S15. Energies (a.u.) and $<S^2>$ values of the BS and T states, and $J/(cm^{-1})$ and H-transfer activation energy barriers ($kcal \cdot mol^{-1}$) of NVH-1-Int and NVH-1-TS from optimization and metadynamics calculations at the B3LYP/6-311G(d,p) level. Among them, the Opt represents the NVH-1-Int and NVH-1-TS were obtained after the geometrical optimization under spin-polarized DFT calculation, and Metad represents the NVH-1-Int1, NVH-1-Int1, and NVH-1-TS were firstly obtained from metadynamics free energy surface and then carried out a single point energy calculations.

Method		E_{BS} ($<S^2>$)	E_T ($<S^2>$)	$J/(cm^{-1})$	Ea/kcal·mol^{-1}
Opt	**Int**	-2721.48776 (0.854)	-2721.48309 (2.008)	-887.61	17.25
	TS	-2721.45844 (1.010)	-2721.46027 (2.011)	401.03	
Metad	**Int-1**	-2721.25725 (0.934)	-2721.25342 (2.008)	-883.00	15.79
	Int-2	-2721.25517 (0.949)	-2721.25122 (2.011)	-909.29	14.48
	TS	-2721.23013(1.012)	-2721.23209 (2.011)	430.59	

Table S16. The distances (Å) of C-C and C-H of NVH-1 in the Int and TS based on the DFT calculation and metadynamics simulation, calculated at the B3LYP/6-311G(d,p) level.

		C_1-H	C_2-H	C_3-H	C_1-C_2	C_1-C_3	C_2-C_3
DFT	Int	1.068	2.020	2.020	2.788	2.788	2.762
	TS	1.372	1.372	2.093	2.596	2.775	2.775
Metad	Int1	1.070	2.015	2.081	2.927	2.889	2.779
	Int2	2.010	1.071	2.106	2.799	2.791	2.691
	TS	1.372	1.372	2.138	2.612	2.798	2.771

		Spin Density	SOMOα1/α	SOMOα2/β
Metad	Int1	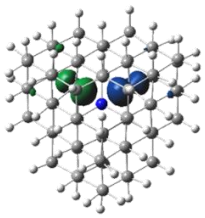	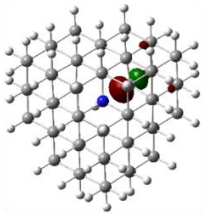	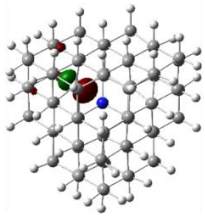
	Int2	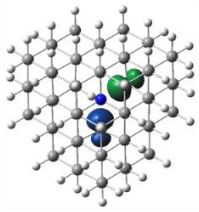	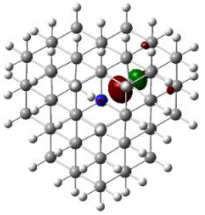	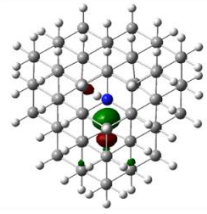
	TS	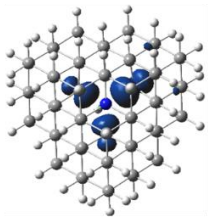	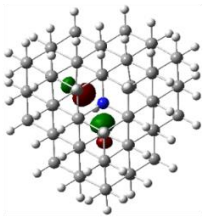	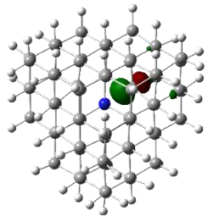

Figure S14. The spin density distributions and singly occupied molecular orbitals (SOMO) of Int1, Int2, and TS on free energy surface.

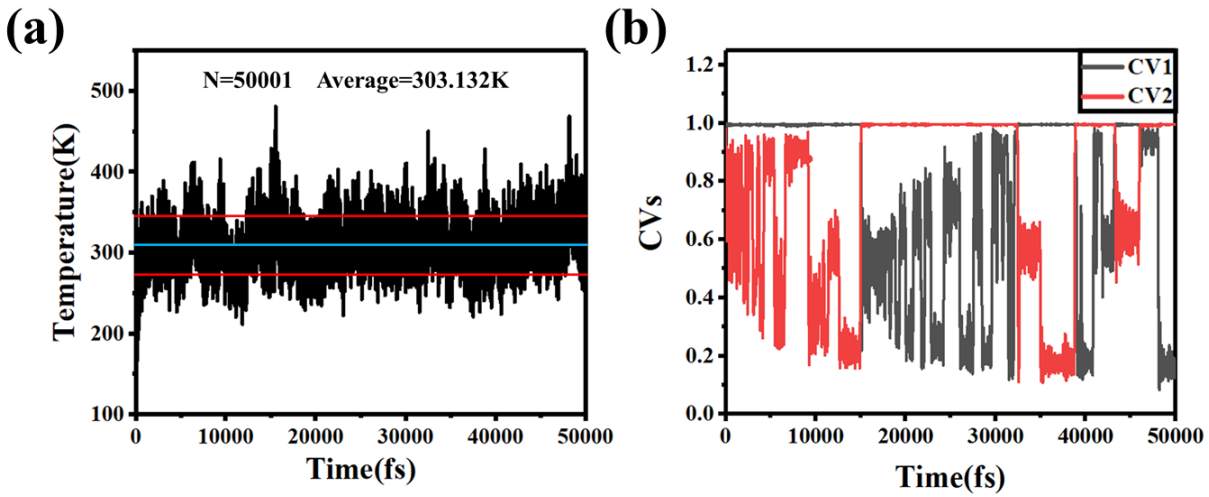

Figure S15. (a) Time evolution of the temperature in metadynamics. **(b)** Evolution of the CVs over the simulation time.

Table S17(A). The magnetic coupling constants along the Int1 and TS regions in Figure 5 (a).

$C_1\cdots H$	$J/(cm^{-1})$	$C_1\cdots H$	$J/(cm^{-1})$	$C_1\cdots H$	$J/(cm^{-1})$
1.065	-1070.16	1.098	-652.91	1.131	-499.37
1.066	-1185.26	1.099	-765.38	1.132	-383.06
1.067	-884.65	1.100	-563.28	1.133	-677.06
1.068	-927.70	1.101	-592.69	1.134	-385.56
1.069	-1176.18	1.102	-760.52	1.135	-385.81
1.070	-939.04	1.103	-469.50	1.136	-903.79
1.071	-1004.96	1.104	-222.47	1.137	-560.02
1.072	-964.51	1.105	-191.92	1.138	-552.21
1.073	-1183.84	1.106	-156.95	1.139	-1281.89
1.074	-1096.63	1.107	-579.27	1.140	-49.00
1.075	-807.76	1.108	-511.63	1.141	-393.18
1.076	-723.43	1.109	-355.81	1.142	-897.40
1.077	-921.30	1.110	-637.49	1.143	-621.97
1.078	-792.98	1.111	-120.93	1.144	-748.82
1.079	-508.62	1.112	-33.79	1.145	-806.42
1.080	-688.83	1.113	-253.28	1.146	-763.61
1.081	-751.85	1.114	-636.25	1.147	-749.93
1.082	-776.73	1.115	-362.45	1.148	-655.86
1.083	-794.17	1.116	-572.54	1.149	-863.49
1.084	-855.55	1.117	-304.35	1.150	-485.30
1.085	-971.61	1.118	-550.81	1.151	-414.55
1.086	-961.24	1.119	-617.05	1.152	-787.06
1.087	-896.57	1.120	-495.19	1.153	-348.57
1.088	-710.62	1.121	-642.05	1.154	-497.35
1.089	-485.70	1.122	-802.09	1.155	-922.74
1.090	-500.55	1.123	-752.90	1.156	-575.09
1.091	-652.95	1.124	-702.46	1.157	-313.00

1.092	-878.71	1.125	-469.05	1.158	-733.30
1.093	-853.00	1.126	-643.75	1.159	-598.25
1.094	-751.82	1.127	-205.11	1.160	-432.23
1.095	-812.83	1.128	-499.08	1.161	-783.80
1.096	-804.98	1.129	-956.78	1.162	-732.45
1.097	-893.64	1.130	-987.81	1.163	-715.54
$C_1\cdots H$	***J*/(cm^{-1})**	**$C_1\cdots H$**	***J*/(cm^{-1})**	**$C_1\cdots H$**	***J*/(cm^{-1})**
1.164	-666.76	1.197	-26.11	1.289	305.44
1.165	-542.81	1.198	-54.01	1.292	210.91
1.166	-731.54	1.199	-78.57	1.295	297.75
1.167	-422.12	1.200	-96.63	1.298	275.04
1.168	-545.75	1.202	40.17	1.301	129.17
1.169	-400.09	1.205	62.04	1.304	200.29
1.170	-346.60	1.208	12.34	1.307	421.02
1.171	-338.78	1.211	53.07	1.310	110.18
1.172	-429.01	1.214	96.66	1.313	291.45
1.173	-424.41	1.217	212.11	1.316	252.11
1.174	-564.95	1.220	171.98	1.319	362.35
1.175	-78.57	1.223	219.06	1.322	187.39
1.176	-190.53	1.226	108.36	1.325	378.24
1.177	-457.35	1.229	55.59	1.328	275.89
1.178	-555.06	1.232	101.23	1.331	237.96
1.179	-475.72	1.235	131.78	1.334	326.28
1.180	-702.59	1.238	141.71	1.337	96.66
1.181	-85.32	1.241	128.54	1.340	478.66
1.182	-88.21	1.244	134.54	1.343	415.72
1.183	-583.22	1.247	74.97	1.346	520.02
1.184	-337.28	1.250	158.53	1.349	587.98
1.185	-587.64	1.253	219.06	1.352	275.89

1.186	-168.19	1.256	128.36	1.355	237.96
1.187	-72.49	1.259	138.91	1.358	387.10
1.188	-91.02	1.262	117.11	1.361	531.01
1.189	-300.28	1.265	142.70	1.364	370.26
1.190	-53.44	1.268	28.38	1.367	519.70
1.191	-210.15	1.271	76.01	1.370	275.04
1.192	-58.27	1.274	102.10	1.373	439.37
1.193	-115.81	1.277	43.92	1.376	342.15
1.194	-182.35	1.280	225.50	1.379	457.94
1.195	-108.64	1.283	289.78	1.382	316.54
1.196	-399.38	1.286	289.52	1.385	597.93

Table S17(B). The structure information of magnetic coupling constants over 900 cm^{-1}.

$C_1\cdots H$	**$C_2\cdots H$**	**$C_1\cdots C_2$**	**$C_2\cdots C_3$**	**$\angle C_1$-H-C_2**	**$\angle$H-C_1-C_2**	***J*/(cm^{-1})**
1.068	2.020	2.788	2.762	126.3	35.7	-887.61(Int)
1.065	1.980	2.702	2.563	123.5	37.7	-1070.16
1.066	2.009	2.762	2.627	126.5	35.8	-1185.26
1.068	2.037	2.759	2.572	123.6	37.9	-927.70
1.069	2.115	2.821	2.575	122.5	39.2	-1176.18
1.070	1.945	2.823	2.494	138.9	26.9	-939.04
1.071	1.862	2.736	2.279	138.1	27.0	-1004.96
1.072	1.899	2.766	2.572	137.3	27.8	-964.51
1.073	1.912	2.679	2.755	126.7	34.9	-1183.84
1.074	2.003	2.732	2.572	123.7	37.6	-1096.63
1.077	1.975	2.630	2.543	127.7	36.9	-921.30
1.085	2.095	2.866	2.605	127.1	35.7	-971.61
1.086	1.981	2.778	2.799	128.9	33.7	-961.24
1.136	1.901	2.726	2.733	127.2	33.7	-903.79
1.139	2.019	2.662	2.729	112.9	44.3	-1281.89
1.155	1.850	2.720	2.620	129.8	31.5	-922.74

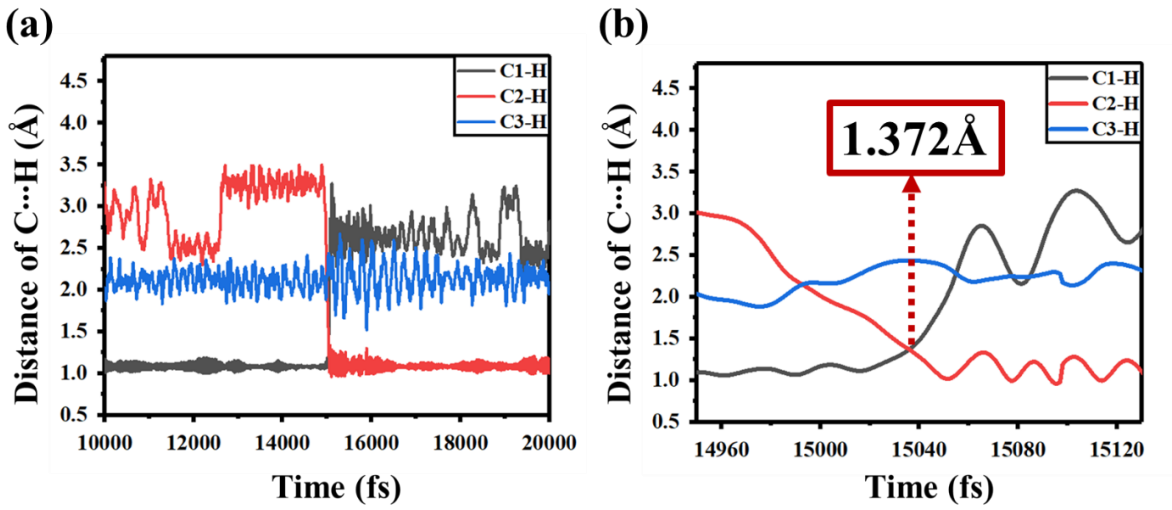

Figure S16. (a) Time evolution of C_1-H/C_2-H/C_3-H distances in the representative intermediate snapshot configurations (10000 fs – 20000 fs) obtained by metadynamics. **(b)** Time evolution of C_1-H/C_2-H/C_3-H distances in the representative intermediate snapshot configurations (14960fs-15120fs) when the H transfers from C_1 to C_2.

Table S18. The distances (Å) of C-H obtained by metadynamics during 14960 – 15120 fs.

Time	C_1-H	C_2-H	C_3-H	Time	C_1-H	C_2-H	C_3-H
14960	1.062	2.961	1.967	15041	1.517	1.259	2.430
14961	1.060	2.956	1.964	15042	1.555	1.234	2.427
14962	1.061	2.950	1.961	15043	1.598	1.208	2.423
14963	1.064	2.943	1.958	15044	1.644	1.180	2.419
14964	1.068	2.935	1.953	15045	1.690	1.151	2.415
14965	1.074	2.925	1.948	15046	1.738	1.121	2.409
14966	1.081	2.914	1.942	15047	1.785	1.092	2.402
14967	1.089	2.901	1.934	15048	1.834	1.065	2.395
14968	1.097	2.885	1.927	15049	1.884	1.043	2.385
14969	1.104	2.868	1.919	15050	1.938	1.027	2.374
14970	1.112	2.848	1.911	15051	1.996	1.018	2.359
14971	1.118	2.826	1.903	15052	2.060	1.019	2.343
14972	1.124	2.802	1.896	15053	2.130	1.028	2.323

14973	1.130	2.775	1.891	15054	2.207	1.046	2.301
14974	1.134	2.746	1.886	15055	2.290	1.069	2.279
14975	1.138	2.714	1.884	15056	2.376	1.096	2.257
14976	1.140	2.679	1.884	15057	2.463	1.125	2.236
14977	1.142	2.642	1.887	15058	2.546	1.156	2.217
14978	1.141	2.603	1.892	15059	2.622	1.188	2.202
14979	1.140	2.562	1.900	15060	2.690	1.220	2.191
14980	1.136	2.520	1.910	15061	2.747	1.250	2.185
14981	1.131	2.478	1.923	15062	2.792	1.278	2.183
14982	1.123	2.437	1.939	15063	2.825	1.302	2.184
14983	1.115	2.397	1.957	15064	2.846	1.321	2.188
14984	1.105	2.360	1.977	15065	2.854	1.332	2.193
14985	1.095	2.325	1.999	15066	2.850	1.336	2.199
14986	1.086	2.293	2.021	15067	2.834	1.331	2.205
14987	1.077	2.264	2.044	15068	2.806	1.318	2.211
14988	1.071	2.240	2.066	15069	2.768	1.297	2.215
14989	1.068	2.217	2.087	15070	2.720	1.268	2.219
14990	1.067	2.197	2.107	15071	2.664	1.232	2.224
14991	1.069	2.178	2.125	15072	2.602	1.189	2.228
14992	1.074	2.161	2.140	15073	2.536	1.142	2.232
14993	1.083	2.143	2.153	15074	2.468	1.095	2.237
14994	1.094	2.126	2.162	15075	2.399	1.052	2.242
14995	1.107	2.108	2.168	15076	2.335	1.018	2.246
14996	1.121	2.090	2.171	15077	2.278	0.998	2.249
14997	1.134	2.072	2.173	15078	2.230	0.996	2.248
14998	1.147	2.052	2.172	15079	2.193	1.012	2.245
14999	1.159	2.032	2.170	15080	2.168	1.043	2.242
15000	1.168	2.014	2.167	15081	2.158	1.081	2.239
15001	1.176	1.996	2.165	15082	2.162	1.122	2.238
15002	1.182	1.979	2.163	15083	2.180	1.160	2.239

15003	1.186	1.963	2.161	15084	2.213	1.191	2.241
15004	1.187	1.948	2.161	15085	2.262	1.212	2.245
15005	1.185	1.934	2.162	15086	2.324	1.223	2.249
15006	1.181	1.921	2.164	15087	2.397	1.221	2.254
15007	1.175	1.908	2.169	15088	2.479	1.207	2.259
15008	1.168	1.896	2.175	15089	2.567	1.181	2.265
15009	1.158	1.883	2.183	15090	2.654	1.145	2.271
15010	1.149	1.872	2.193	15091	2.738	1.103	2.278
15011	1.140	1.860	2.205	15092	2.817	1.057	2.286
15012	1.131	1.848	2.217	15093	2.890	1.014	2.294
15013	1.124	1.836	2.231	15094	2.956	0.981	2.299
15014	1.118	1.823	2.246	15095	3.017	0.963	2.299
15015	1.115	1.809	2.260	15096	3.071	0.963	2.293
15016	1.114	1.795	2.275	15097	3.120	0.981	2.279
15017	1.116	1.780	2.290	15098	3.163	1.190	2.174
15018	1.121	1.763	2.306	15099	3.200	1.225	2.159
15019	1.128	1.744	2.321	15100	3.230	1.253	2.148
15020	1.138	1.725	2.335	15101	3.252	1.271	2.142
15021	1.149	1.704	2.348	15102	3.266	1.281	2.140
15022	1.162	1.682	2.360	15103	3.274	1.281	2.142
15023	1.175	1.658	2.372	15104	3.274	1.272	2.149
15024	1.189	1.633	2.383	15105	3.268	1.255	2.160
15025	1.202	1.608	2.392	15106	3.256	1.230	2.175
15026	1.215	1.583	2.401	15107	3.240	1.199	2.195
15027	1.228	1.558	2.409	15108	3.219	1.162	2.218
15028	1.242	1.534	2.416	15109	3.195	1.123	2.245
15029	1.255	1.511	2.422	15110	3.167	1.084	2.274
15030	1.269	1.489	2.427	15111	3.137	1.047	2.303
15031	1.283	1.468	2.432	15112	3.104	1.018	2.331
15032	1.297	1.447	2.435	15113	3.067	1.001	2.355

15033	1.313	1.426	2.437	15114	3.025	0.997	2.374
15034	1.331	1.407	2.439	15115	2.980	1.007	2.387
15035	1.351	1.387	2.440	15116	2.932	1.030	2.395
15036	1.372	1.372	2.440	15117	2.881	1.062	2.398
15037	1.395	1.348	2.439	15118	2.831	1.098	2.400
15038	1.421	1.327	2.438	15119	2.784	1.135	2.399
15039	1.449	1.305	2.436	15120	2.742	1.169	2.398
15040	1.481	1.282	2.433	15121	2.707	1.198	2.395

8. Magnetic Coupling Distributions from Scanning

Qualitative Expression of Magnetic Characteristics. To further understand the magnetic characteristics during the H transferring in the tetrahedral defect space within the NVH center, a visual qualitative representation of the magnetic properties is presented next, which is mainly from three perspectives.

Firstly, because of the equivalence of three C-radicals, we just analyzed the magnetic characteristics of the H transferred within half of the $\angle C_2$-C_1-C_3 sector, corresponding to one-sixth of this triangular region (Figure S17 (a)), as a presentation of the magnetic characteristics within the entire triangular region for NVH center. We carried out two-dimensional scans with the symmetry of the structure taken into account, where the $C_1\cdots H$ distance was scanned from 1.0-1.4 Å with an increment of 0.05 Å and the angle $\angle$H-C_1-C_2 was scanned from 15-40° with an increment of 5°. In total, 54 points were scanned into the data set in this way. And then, to get the magnetic coupling constants *J* of the NVH center, single-point energies of the BS state and T state for 54 structures were calculated.

Figure S17 (b) shows that the energy is the lowest when the H is around the bonding distance (1.081 Å for NVH-Int) and the angle of $\angle$H-C_1-C_2 is near 40° when the projection of the C_1-H bond is almost in the middle of $\angle C_2$-C_1-C_3 (37.1° for NVH-Int). The energy of the cluster gradually increases as the $C_1\cdots H$ distance increases (1.0 Å $\rightarrow$ 1.4 Å) and the $\angle$H-C_1-C_2 decreases (40° $\rightarrow$ 15°). The magnetic coupling constants are increased, i.e., AFM is apparently weakened and FM is gradually strengthened as the $C_1\cdots H$ distance and the $\angle$H-C_1-C_2 increase (Figure

S17(c)). When the $C_1\cdots H$ distance is up to 1.4 Å and the $\angle H\text{-}C_1\text{-}C_2$ is up to 40° (the projection of the H is almost in the center of the triangular plane composed of $C_1\text{-}C_2\text{-}C_3$), the magnetic property of NVH changes from AFM to FM. In a word, within the fan-shaped region close to one-sixth of this triangular enclosed by three C-radicals, the NVH center would prefer to present AFM characteristics, and at the center region of the triangular, the NVH center may tend to show FM property. Next two perspectives we explored the magnetism property by changing the $C_1\cdots H$ and $N\cdots H$ distance, respectively, i.e., one-dimensional scans.

Secondly, another variation distance is $C_1\cdots H$ with the fixed $\angle H\text{-}C_1\text{-}C_2$ at 40°. The method is taking the NVH-Int as the initial structure and gradually changes the distance of $C_1\cdots H$ by scanning. According to the metadynamics, the minimum distance of $C\cdots H$ telescopic vibration reached 0.963 Å, and when the distance of $C_1\cdots H$ is almost through the plane of $N\text{-}C_2\text{-}C_3$, the $C_1\cdots H$ distance is at about 2.7 Å for NVH-0 and 2.4 Å for NVH-1. Thus, to observe the magnetism property over a wide range of $C_1\cdots H$ distances, we calculated the *J* by scanning the $C_1\cdots H$ distance from 0.9 Å to 2.8 Å. Though the very short and the very long $C_1\cdots H$ distance may be difficult to obtain, the possibilities of H tunneling to certain spatial locations may exist. And our calculations here only want to qualitatively express the magnetic state of the H at these locations. Thus, this distance range we think is acceptable. Based on the above principles, we calculated all the magnetic coupling constants of NVH-0 and NVH-1 at different $C_1\cdots H$ distances. The FM strength increases monotonically as the $C_1\cdots H$ distance increases, and the FM strength starts to decrease when the distance of $C_1\cdots H$ is through the plane of $N\text{-}C_2\text{-}C_3$. However, in this case, the H is no longer in the tetrahedral space composed of $N\text{-}C_1\text{-}C_2\text{-}C_3$ and is not considered. (Figure S18(a)-(b)). The turning point of AFM to FM is at the $C_1\cdots H$ distance of 1.4 Å which is consistent with the result we obtained from the two-dimensional scans in the last part. However, according to our previous description of the IRC results, the molecule has exhibited FM characteristics when the $C_1\cdots H$ distance reaches 1.4 Å, whereas here it has just reached the turning point between AFM and FM. This is mainly due to the angle of the $\angle H\text{-}C_1\text{-}C_2$ continuously decreasing from the initial state to TS (37.1°→18.8° for NVH-0, and 35.7°→18.9° for NVH-1) in the IRC approach rather than fixed as the one-dimensional scans (Table S8). Since it does not affect the focus of this part of our discussion, it will not be discussed.

Thirdly, the last part discussion of the magnetic coupling is based on the H in the region above but close to the C_1-C_2-C_3 plane. However, what about the magnetic properties when the H is far from this plane and extremely near this plane? To simplify the calculation work, we just choose the structures when the projection of the H is located in the center of the triangular C_1-C_2-C_3 plane. Similar to the choice of the $C_1\cdots H$ distance variation, we calculated the magnetic coupling constants for the corresponding structures of NVH-0 and NVH-1 at different N···H distances changing from 0.9 Å to 2.3 Å. According to the metadynamics, the minimum distance of N···H telescopic vibration reached 0.930 Å. And the distance of N···H is 2.1 Å when the H is on the triangular C_1-C_2-C_3 plane. Similarly, the very short and the very long N···H distances of the cluster may be difficult to obtain, but the possibilities of H tunneling to certain spatial locations may exist. The total variation of magnetic coupling constants of NVH-0 and NVH-1 is shown in Figure S18 which both exhibit strong FM character with the N···H distance increasing. The magnetism strength is weakening when the H crosses the C_1-C_2-C_3 plane or is very close to the N, which is similar to the case of the last part. All these results may indicate that the magnetism strength will be weakened after the H crosses this inner tetrahedral space.

Obviously, the calculated magnetic strength in the above discussions is significantly enhanced compared to the initial state and TS structures, except for the normal $C_1\cdots H$ distances range between Int (~1.0 Å) and TS (~1.4 Å). This issue can be better understood in terms of the energies of these structures. Results show that $|\Delta E_{BS\text{-}T}|$ is much larger than that of the initial state and TS structures when changing the $C_1\cdots H$ and N···H distances, which makes the magnetic coupling constants of the corresponding structures much larger than that (Figure 19 (a) &(b)). Although the clusters in these states have stronger AFM or FM, it is of concern that the energy required for H to migrate to these positions is also conceivably high. As shown in Figure 19 (c), the energy barriers are all over 30 kcal·mol^{-1} when the $C_1\cdots H$ distances are longer than 1.4 Å. Similarly, the energy barriers are all over 50 kcal•mol^{-1} when H is away from the three C-sites at different N···H distances. Above all, we qualitatively obtained the magnetic properties, but how to control the stable presence of the H in these regions with higher potential barriers to obtain stronger magnetic characteristics is yet to be solved.

Finally, we qualitatively expressed the magnetic characteristics when the H is located in different projection positions of the triangular C_1-C_2-C_3 plane. In the sector of the H near either three C-radicals, the NVH center will exhibit AFM. When the H is located in the central region, it will exhibit FM. The white curve represents the H transfer path projection along the IRC path.

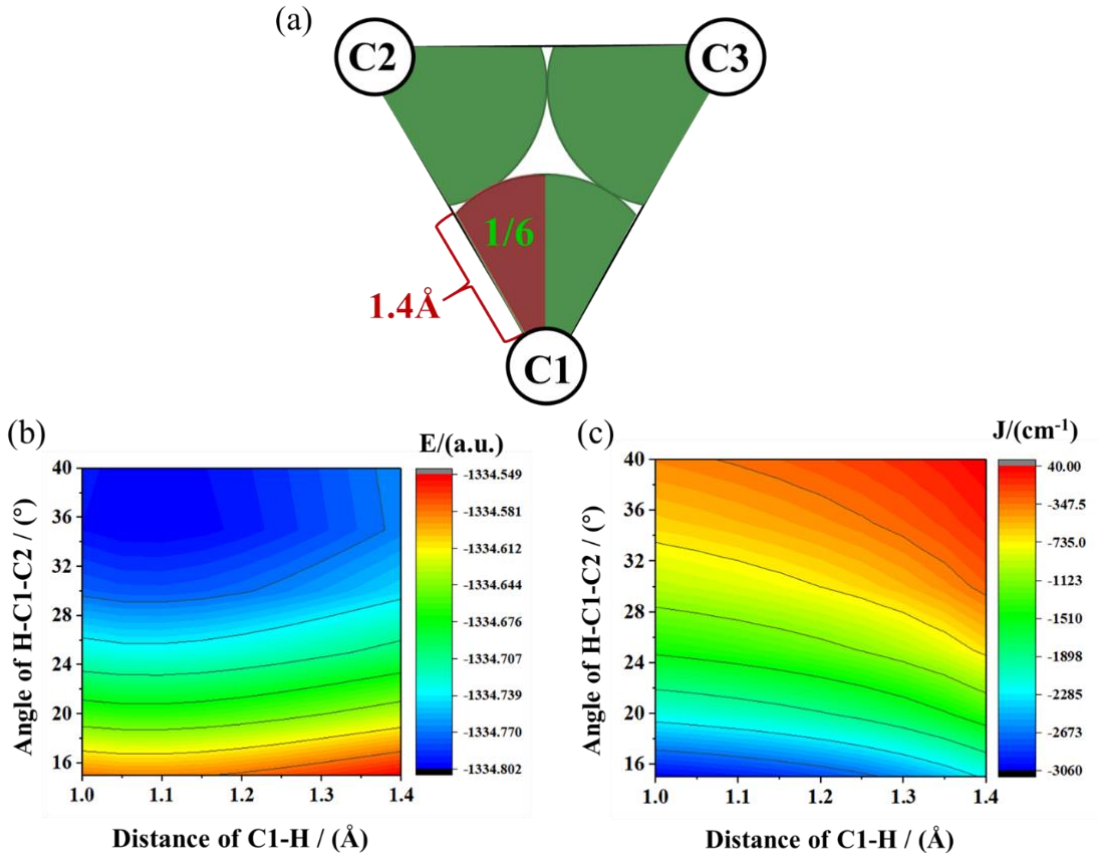

Figure S17. (a) The 1/6 represents the scanning area projection with the $C_1\cdots H$ distance changing from 1.0 Å to 1.4 Å and the $\angle H\text{-}C_1\text{-}C_2$ changing from 15° to 40° of NVH-0. The $\angle H\text{-}C_1\text{-}C_2$ at 40° corresponds to the projection of $C_1\cdots H$ in the middle of $\angle C_2\text{-}C_1\text{-}C_3$, and at 15° the projection of $C_1\cdots H$ almost overlaps with the $C_1\cdots C_2$ line. 3D projection of the (b) energies and (c) magnetic coupling constants at the scanning region.

Table S19(A). Energies (a.u.) at the scanning region of NVH-0.

	15°	20°	25°	30°	35°	40°
1.00 Å	-1334.58080	-1334.66055	-1334.72769	-1334.77437	-1334.79690	-1334.79487
1.05 Å	-1334.58463	-1334.66448	-1334.73172	-1334.77849	-1334.80108	-1334.79909
1.10 Å	-1334.58469	-1334.66466	-1334.73201	-1334.77885	-1334.80149	-1334.79956
1.15 Å	-1334.58195	-1334.66206	-1334.72954	-1334.77644	-1334.79913	-1334.79724
1.20 Å	-1334.57719	-1334.65747	-1334.72506	-1334.77203	-1334.79476	-1334.79291
1.25 Å	-1334.57105	-1334.65150	-1334.71920	-1334.76621	-1334.78896	-1334.78715
1.30 Å	-1334.56405	-1334.64468	-1334.71245	-1334.75947	-1334.78221	-1334.78042
1.35 Å	-1334.55663	-1334.63744	-1334.70524	-1334.75220	-1334.77487	-1334.77308
1.40 Å	-1334.54921	-1334.63016	-1334.69790	-1334.74469	-1334.76723	-1334.76557

Table S19(B). Magnetic coupling constants (J/cm^{-1}) at the scanning region of NVH-0.

	15°	20°	25°	30°	35°	40°
1.00 Å	-3050.82	-2167.66	-1458.44	-963.76	-636.25	-401.65
1.05 Å	-3011.79	-2121.30	-1409.65	-917.74	-594.97	-366.13
1.10 Å	-2963.58	-2065.52	-1352.48	-864.82	-548.33	-327.08
1.15 Å	-2903.64	-1998.20	-1285.53	-803.62	-495.72	-283.44
1.20 Å	-2828.24	-1916.35	-1206.38	-733.01	-436.36	-234.87
1.25 Å	-2732.56	-1815.66	-1111.26	-650.77	-368.95	-181.03
1.30 Å	-2610.38	-1690.19	-995.39	-553.44	-290.97	-120.43
1.35 Å	-2453.40	-1532.62	-853.55	-436.19	-198.77	-50.44
1.40 Å	-2250.66	-1334.37	-679.14	-293.00	-87.48	32.30

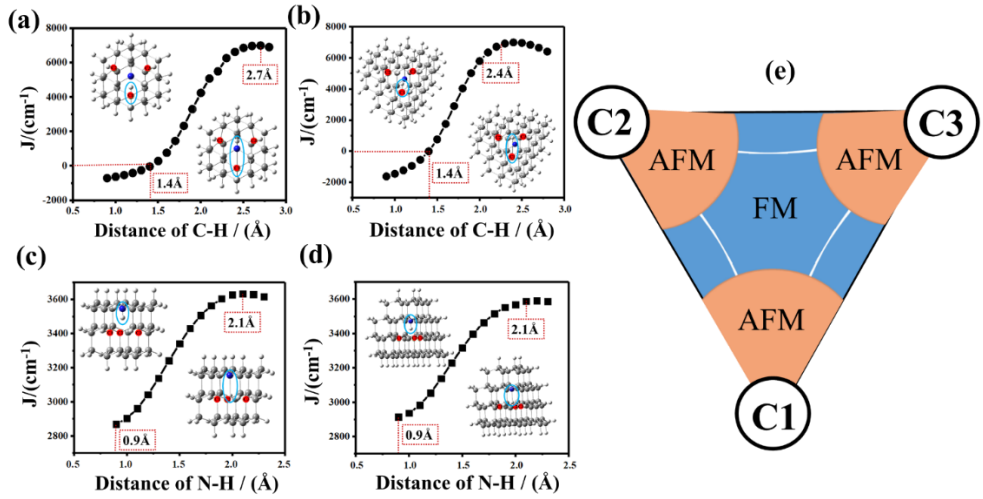

Figure S18. Magnetic coupling constants of the (a) NVH-0 and (b) NVH-1 at different C···H distances when extend this C···H distance along the point of H to reach the opposite triangle. Magnetic coupling constants of the (c) NVH-0 and (d) NVH-1 at different N···H distances when the projection of H is centered in the triangle formed by C_1-C_2-C_3. (e) Schematic representation of the magnetic characteristics of the NVH center when the projection of H is located in different regions of the triangle formed by C_1-C_2-C_3, where the white curve represents FM region projection when the H transferring along the IRC path.

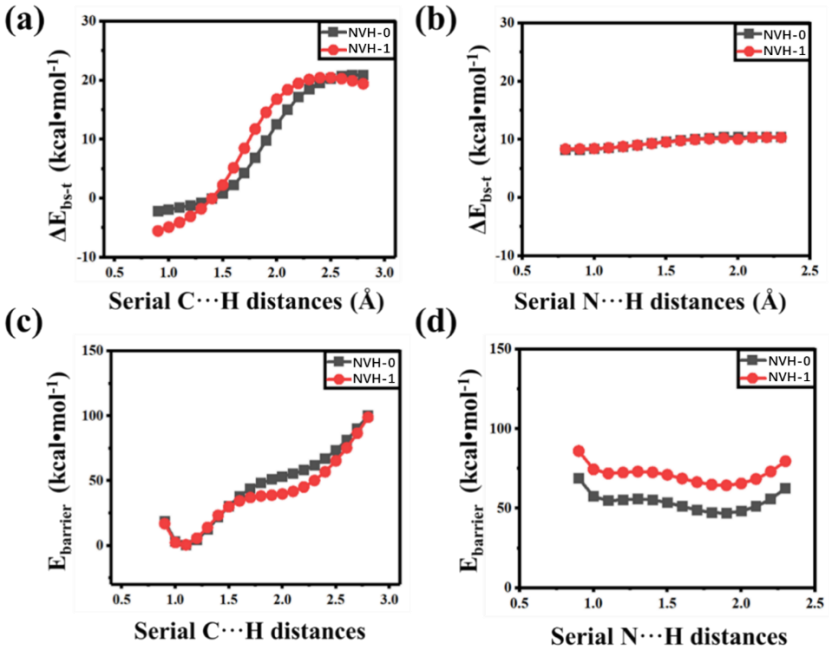

Figure S19. Energy differences of BS and T states ($\Delta E_{BS\text{-}T}$, kcal·mol^{-1}) at different (a) C···H and (b) N···H distances of NVH-0 and NVH-1. Energy differences between structures in different (c) C···H and (d) N···H distances and the initial state ($E_{barrier}$, kcal·mol^{-1}) of NVH-0 and NVH-1.

Table S20(A). Energies and $<S^2>$ values of the BS and T states, and *J*, calculated at the B3LYP/6-311G(d,p) level at different $C_1\cdots H$ distances of NVH-0. ΔE_{BS-T} represents the energy difference between BS and T states, and $E_{barrier}$ represents the energy difference between NVH-0 at different $C_1\cdots H$ distances and the initial state.

Distance of C_1-H(Å)	E_{BS}/a.u. ($<S^2>$)	E_T/a.u. ($<S^2>$)	ΔE_{BS-T} (kcal·mol^{-1})	$E_{barrier}$ (kcal·mol^{-1})	*J*/(cm^{-1})
0.6	-1334.35412 (0.920)	-1334.34987 (2.009)	-2.668	282.303	-856.67
0.7	-1334.58957 (0.924)	-1334.58552 (2.009)	-2.543	134.556	-819.67
0.8	-1334.71306 (0.929)	-1334.70928 (2.009)	-2.376	57.063	-769.87
0.9	-1334.77390 (0.936)	-1334.77044 (2.009)	-2.167	18.891	-706.54
1.0	-1334.79895 (0.944)	-1334.79591 (2.009)	-1.912	3.167	-627.73
1.1	-1334.80358 (0.952)	-1334.80103 (2.009)	-1.601	0.261	-529.86
1.2	-1334.79689 (0.962)	-1334.79495 (2.009)	-1.220	4.460	-407.38
1.3	-1334.78436 (0.972)	-1334.78318 (2.009)	-0.737	12.326	-248.51
1.4	-1334.76936 (0.982)	-1334.76922 (2.011)	-0.088	21.739	-30.06
1.5	-1334.75402 (0.992)	-1334.75537 (2.014)	0.846	30.514	289.54
1.6	-1334.73968 (1.000)	-1334.74326 (2.021)	2.246	38.115	769.54
1.7	-1334.72702 (1.006)	-1334.73382 (2.030)	4.266	44.038	1456.22
1.8	-1334.71627 (1.008)	-1334.72721 (2.038)	6.864	48.187	2331.64
1.9	-1334.70723 (1.007)	-1334.72277 (2.040)	9.752	50.971	3302.13
2.0	-1334.69937 (1.006)	-1334.71938 (2.040)	12.555	53.099	4248.29
2.1	-1334.69198 (1.005)	-1334.71589 (2.038)	15.001	55.290	5080.15
2.2	-1334.70636 (1.029)	-1334.71138 (2.036)	17.149	58.121	5508.53

2.3	-1334.67579 (1.005)	-1334.70522 (2.035)	18.465	61.986	6269.32
2.4	-1334.66593 (1.005)	-1334.69706 (2.035)	19.535	67.105	6631.66
2.5	-1334.65449 (1.004)	-1334.68677 (2.037)	20.254	73.563	6861.17
2.6	-1334.64143 (1.003)	-1334.67439 (2.040)	20.683	81.329	6974.30
2.7	-1334.66044 (1.071)	-1334.66012 (2.047)	20.883	90.287	7012.34
2.8	-1334.61102 (0.999)	-1334.64429 (2.056)	20.877	100.219	6906.51

Table S20(B). Energies and $<S^2>$ values of the BS and T states, and *J*, calculated at the B3LYP/6-311G(d,p) level at different $C_1\cdots H$ distances of the NVH-1. ΔE_{BS-T} represents the energy difference between BS and T states, and $E_{barrier}$ represents the energy difference between the NVH-1 in different $C_1\cdots H$ distances and the initial state.

Distance of C_1-H(Å)	**E_{BS}/a.u. ($<S^2>$)**	**E_T/a.u. ($<S^2>$)**	**ΔE_{BS-T} (kcal·mol^{-1})**	**$E_{barrier}$ (kcal·mol^{-1})**	***J*/(cm^{-1})**
0.6	-2721.04601 (0.782)	-2721.03521 (2.008)	-6.774	277.355	-1932.12
0.7	-2721.28016 (0.792)	-2721.26986 (2.008)	-6.464	130.421	-1859.20
0.8	-2721.40206 (0.805)	-2721.39242 (2.008)	-6.053	53.926	-1759.94
0.9	-2721.46106 (0.821)	-2721.45225 (2.008)	-5.531	16.904	-1629.66
1.0	-2721.48424 (0.839)	-2721.47646 (2.008)	-4.882	2.362	-1461.34
1.1	-2721.48713 (0.861)	-2721.48064 (2.008)	-4.077	0.544	-1242.85
1.2	-2721.47906 (0.884)	-2721.47417 (2.008)	-3.066	5.610	-954.40
1.3	-2721.46577 (0.911)	-2721.46295 (2.009)	-1.767	13.951	-562.59
1.4	-2721.45089 (0.938)	-2721.45081 (2.011)	-0.045	23.290	-14.54
1.5	-2721.43678 (0.963)	-2721.44037 (2.015)	2.254	29.886	749.66

1.6	-2721.42482 (0.984)	-2721.43307 (2.019)	5.172	34.471	1746.94
1.7	-2721.41547 (0.997)	-2721.42898 (2.021)	8.474	37.037	2892.67
1.8	-2721.40844 (1.003)	-2721.42715 (2.021)	11.736	38.186	4030.45
1.9	-2721.40293 (1.004)	-2721.42614 (2.020)	14.564	38.820	5016.48
2.0	-2721.39785 (1.004)	-2721.42460 (2.018)	16.787	39.784	5789.94
2.1	-2721.39215 (1.003)	-2721.42148 (2.017)	18.400	41.745	6347.98
2.2	-2721.38505 (1.002)	-2721.41610 (2.016)	19.479	45.120	6713.89
2.3	-2721.37600 (0.999)	-2721.40807 (2.016)	20.126	50.154	6919.14
2.4	-2721.36476 (0.995)	-2721.39732 (2.017)	20.428	56.905	6991.86
2.5	-2721.35127 (0.989)	-2721.38387 (2.018)	20.458	65.342	6958.03
2.6	-2721.33562 (0.983)	-2721.36793 (2.019)	20.275	75.346	6838.44
2.7	-2721.31819 (0.975)	-2721.34993 (2.022)	19.915	86.641	6648.98
2.8	-2721.29944 (0.966)	-2721.33037 (2.026)	19.408	98.912	6402.41

Table S20(C). Energies and $<S^2>$ values of the BS and T states, and *J*, calculated at the B3LYP/6-311G(d,p) level at different N···H distances of the NVH-0. ΔE_{BS-T} represents the energy difference between BS and T states, and $E_{barrier}$ represents the energy difference between the NVH-0 in different N···H distances and the initial state.

Distance of N-H (Å)	**E_{BS}/a.u. ($<S^2>$)**	**E_T/a.u. ($<S^2>$)**	**ΔE_{BS-T} (kcal·mol^{-1})**	**$E_{barrier}$ (kcal·mol^{-1})**	***J*/(cm^{-1})**
0.5	-1333.82799 (1.008)	-1333.84120 (2.011)	8.295	604.164	2892.33
0.6	-1334.27178 (1.008)	-1334.28492 (2.011)	8.246	325.725	2875.03
0.7	-1334.49528 (1.007)	-1334.50836 (2.011)	8.207	185.518	2861.37

0.8	-1334.60469 (1.007)	-1334.61875 (2.011)	8.197	116.875	2857.42
0.9	-1334.65378 (1.007)	-1334.66690 (2.011)	8.233	86.031	2869.29
1.0	-1334.67196 (1.007)	-1334.68524 (2.011)	8.333	74.522	2902.71
1.1	-1334.67579 (1.006)	-1334.68935 (2.011)	8.506	71.946	2960.71
1.2	-1334.67455 (1.006)	-1334.68849 (2.012)	8.746	72.483	3041.47
1.3	-1334.67307 (1.006)	-1334.68747 (2.013)	9.032	73.127	3137.98
1.4	-1334.67331 (1.006)	-1334.68818 (2.013)	9.333	72.675	3240.68
1.5	-1334.67543 (1.006)	-1334.69077 (2.013)	9.625	71.051	3340.97
1.6	-1334.67869 (1.006)	-1334.69444 (2.013)	9.883	68.747	3430.93
1.7	-1334.68197 (1.006)	-1334.69806 (2.013)	10.099	66.478	3506.41
1.8	-1334.68426 (1.006)	-1334.70061 (2.013)	10.262	64.879	3563.74
1.9	-1334.68471 (1.006)	-1334.70124 (2.013)	10.376	64.480	3603.81
2.0	-1334.68281 (1.006)	-1334.69945 (2.013)	10.445	65.606	3627.10
2.1	-1334.67824 (1.006)	-1334.69491 (2.013)	10.458	68.455	3632.54
2.2	-1334.67052 (1.007)	-1334.68746 (2.014)	10.456	73.130	3629.58
2.3	-1334.661 (1.007)	-1334.67714 (2.015)	10.428	79.608	3616.39

Table S20(D). Energies and $<S^2>$ values of the BS and T states, and *J*, calculated at the B3LYP/6-311G(d,p) level at different N···H distances of the NVH-1. ΔE_{BS-T} represents the energy difference between BS and T states, and $E_{barrier}$ represents the energy difference between the NVH-1 in different N···H distances and the initial state.

Distance of N-H (Å)	**E_{BS}/a.u. ($<S^2>$)**	**E_T/a.u. ($<S^2>$)**	**ΔE_{BS-T} (kcal·mol^{-1})**	**$E_{barrier}$ (kcal·mol^{-1})**	***J*/(cm^{-1})**

0.5	-2720.53946 (1.007)	-2720.55305 (2.009)	8.526	586.693	2973.79
0.6	-2720.98321 (1.007)	-2720.99668 (2.009)	8.450	308.307	2947.43
0.7	-2721.20659 (1.007)	-2721.21996 (2.009)	8.386	168.199	2924.63
0.8	-2721.31589 (1.006)	-2721.32920 (2.009)	8.349	99.651	2911.21
0.9	-2721.36492 (1.006)	-2721.37824 (2.010)	8.357	68.875	2913.18
1.0	-2721.38308 (1.006)	-2721.39651 (2.010)	8.427	57.413	2936.24
1.1	-2721.38695 (1.006)	-2721.40061 (2.010)	8.569	54.840	2983.32
1.2	-2721.38584 (1.006)	-2721.40061 (2.011)	8.776	55.333	3052.61
1.3	-2721.38454 (1.006)	-2721.39893 (2.012)	9.027	55.894	3137.35
1.4	-2721.38501 (1.005)	-2721.40061 (2.012)	9.294	55.335	3228.34
1.5	-2721.38735 (1.005)	-2721.40257 (2.013)	9.552	53.607	3317.20
1.6	-2721.39078 (1.005)	-2721.40637 (2.012)	9.782	51.224	3397.24
1.7	-2721.39417 (1.005)	-2721.41006 (2.012)	9.972	48.909	3464.06
1.8	-2721.39648 (1.005)	-2721.41260 (2.012)	10.118	47.313	3515.62
1.9	-2721.39689 (1.005)	-2721.41318 (2.012)	10.224	46.951	3552.28
2.0	-2721.39500 (1.005)	-2721.41100 (2.012)	10.040	48.318	3563.38
2.1	-2721.39008 (1.006)	-2721.40654 (2.013)	10.331	51.116	3587.66
2.2	-2721.38241 (1.006)	-2721.39890 (2.014)	10.347	55.910	3590.61
2.3	-2721.37181 (1.006)	-2721.38829 (2.015)	10.345	62.566	3585.80